

REPORT DOCUMENTATION PAGE

1. IDENTIFICATION NUMBER AD-A201 425		2b. RESTRICTIVE MARKINGS OTIC FILE COPY	
3. DISTRIBUTION / AVAILABILITY OF REPORT Approved for public release; distribution is unlimited.		4. PERFORMING ORGANIZATION REPORT NUMBER(S) D 8	
5. MONITORING ORGANIZATION REPORT NUMBER(S) AFOSR-TR- 88-1292		6a. NAME OF PERFORMING ORGANIZATION Univ of Rochester	
6b. OFFICE SYMBOL (if applicable)		7a. NAME OF MONITORING ORGANIZATION AFOSR/NP	
6c. ADDRESS (City, State, and ZIP Code) 518 Hylan Building Rochester, NY 14627		7b. ADDRESS (City, State, and ZIP Code) Building 410, Bolling AFB DC 20332-6448	
8a. NAME OF FUNDING / SPONSORING ORGANIZATION AFOSR		8b. OFFICE SYMBOL (if applicable) NP	
9. PROCUREMENT INSTRUMENT IDENTIFICATION NUMBER AFOSR-84-0175		10. SOURCE OF FUNDING NUMBERS	
8c. ADDRESS (City, State, and ZIP Code) Building 410, Bolling AFB DC 20332-6448		PROGRAM ELEMENT NO. 61102F	PROJECT NO. 2301
		TASK NO. A7	WORK UNIT ACCESSION NO.
11. TITLE (Include Security Classification) (U) INVESTIGATION OF THE PERFORMANCE OF PHOTOCONDUCTIVE SWITCHES			
12. PERSONAL AUTHOR(S) Dr William R. Donaldson			
13a. TYPE OF REPORT Final	13b. TIME COVERED FROM 1 Jul 84 to 30 Jun 88	14. DATE OF REPORT (Year, Month, Day) Sept 1988	15. PAGE COUNT 58
16. SUPPLEMENTARY NOTATION			
17. COSATI CODES		18. SUBJECT TERMS (Continue on reverse if necessary and identify by block number)	
FIELD	GROUP	SUB-GROUP	
	20.12		
19. ABSTRACT (Continue on reverse if necessary and identify by block number) <p>The investigators have shown that photoconductive switches can be used to activate a switch in a radial transmission line geometry. The structure investigated, has demonstrated gain in approximate agreement with theoretical predictions and the device may be useful as an accelerating element in a compact accelerator. They have shown that repetitive opening switches can be constructed from optically activated ceramic superconductors.</p>			
20. DISTRIBUTION / AVAILABILITY OF ABSTRACT <input checked="" type="checkbox"/> UNCLASSIFIED/UNLIMITED <input type="checkbox"/> SAME AS RPT. <input type="checkbox"/> OTIC USERS		21. ABSTRACT SECURITY CLASSIFICATION UNCLASSIFIED	
22a. NAME OF RESPONSIBLE INDIVIDUAL B L SMITH		22b. TELEPHONE (Include Area Code) (202) 767-4908	22c. OFFICE SYMBOL AFOSR/NP

AFOSR-TR- 88 - 1292

INVESTIGATION OF THE PERFORMANCE OF PHOTOCONDUCTIVE SWITCHES

Final Technical Report to the Air Force Office of Scientific Research

Dr. William R. Donaldson

Contract # AFOSR-84-0175

AIR FORCE OFFICE OF SCIENTIFIC RESEARCH (AFOSR)
NOTICE OF TRANSMITTAL TO DTIC
This technical report has been reviewed and is approved for public release IAW AFR 190-12.
Distribution is unlimited.
MATTHEW J. KERPER
Chief, Technical Information Division

Approved for public release;
distribution unlimited.

INTRODUCTION

In the picosecond time domain, photoconductive switches provide a unique and versatile method of switching high voltages. A pulsed biased photoconductive switch can withstand 50 kV in the open state. The same switch, depending on the circuit geometry and laser pulse width, can close in 1 to 300 ps. The speed and voltage handling capability of a photoconductive switch is unmatched by any other device.

A photoconductive switch closes by the generation of electron-hole pairs throughout the volume of the semiconductor material. The bulk activation of the switch eliminates statistical processes such as avalanching that can introduce temporal jitter in the electrical signal. The lack of temporal jitter between the electrical and optical pulses enables us to trigger several switches with a single optical pulse. The combined electrical pulses will have a jitter that is only a few percent of the optical pulse width. In addition, the optical activation of the switch provides electrical isolation between the trigger circuit and the high voltage network. The geometry of these switches is very flexible. Any geometry for which an optical system can be designed to deliver the laser energy to the semiconductor is acceptable.

To achieve the advantages listed above, the electrical switching system must be coupled to a short pulse, high energy laser. This can significantly increase the complexity of the system. The fastest rise times with the minimum laser energy requires that the photoconducting gap in the semiconductor be as small as possible. Thus, to avoid premature electrical breakdown and the possibility of thermal runaway in materials such as



A-1

silicon which have low resistivity, the switch must be pulsed biased. The photoconductive switches do not eliminate the need for conventional elements in a pulse forming network (PFN). Instead the switch will generally act as pulse sharpening element in a larger PFN.

During the course of this contract, we explored the techniques necessary to achieve high voltage switching on the picosecond time scale. This report describes the lasers and PFN's necessary to drive picosecond photoconductive switches. The circuits which incorporate these switches must be designed so as to preserve the large amplitude, high bandwidth electrical pulses that are generated with these switches. A variety of circuits that we constructed to accomplish this are described. This report also describes the electro-optic measuring techniques we use to characterize the behavior of these switches.

LASER SYSTEM

Ultrafast, photoconductive switching cannot be done without an appropriate laser system. The high energy, short-pulse laser systems used for these experiments all relied on a lasing medium incorporating a Nd^{+3} ion in a solid state host producing radiation at about $1.06 \mu\text{m}$. This wavelength is well suited for photoconductive switches. Its absorption depth in Si and GaAs (due to EL2 traps and deep levels associated with the chromium doping) closely matches the skin depth of the electrical frequencies that are generated in the switch.^{1,2}

The lasers used in these experiments were capable of supplying optical energies of between $200 \mu\text{J}$ to 2mJ in pulses with durations from 3ps to 200ps . The laser systems were based on the concept of a regenerative amplifier as illustrated in Fig. 1. A single pulse from a mode-locked oscillator (50ps to 200ps) was injected into a Q-switched laser cavity used as an amplifier. The injection seeding of the amplifier produced pulses with energies up to 2mJ and pulse durations equal to the injected pulse duration. The Q-switching and injection were accomplished with a Pockels cell to electronically rotate the optical polarization in the cavity.

To access the shortest pulse durations, additional pulse compression techniques were applied. The pulsed laser used in these investigations was a combination of a Nd:YLF oscillator and a Nd:glass amplifier ($\lambda = 1.054 \mu\text{m}$), producing pulses of a few millijoules of 1 ps to 3 ps duration at a repetition rate of 5 Hz.³ The short, low energy optical pulse was stretched in time and given a frequency chirp before being injected into the amplifier. This was done by passing the light through an optical fiber. Self-phase modulation in the fiber increased the spectral width of the pulse allowing the full gain bandwidth of the lasing medium to be exploited. The self-phase modulation combined with group velocity dispersion gives the pulse a frequency chirp that it maintains throughout the amplification processes. The amplified pulse propagated through a dispersive delay line formed by a matched grating pair. This line had a dispersive characteristic of the opposite sign from the original fiber dispersion. Thus, the amplified pulse could be compressed to a pulse shorter than the original pulse from the oscillator. The advantage is that the peak optical power in the amplifier is greatly reduced. Thus, the size of the optical components can be reduced without being subject to optical damage. The longer pulse is also much more efficient at extracting energy from the subsequent amplifying stages.

The size of the optical system is determined by the amount of optical energy it must supply. This is dictated by the size of the photoconductive switch. Each optical photon generates a single electron hole pair, with no additional carriers being generated by other mechanisms. To achieve optimal switching, the semiconductor must obtain a carrier density of at least 10^{16} per cm^3 . The absorption depth of the $1 \mu\text{m}$ radiation is roughly 1 mm at room temperature. This depth establishes the effective thickness of the semiconductor. The width of the gap is determined by the voltage that the switch must withstand and the transverse length of the switch is established by the maximum current the switch must handle. Silicon can carry 1.35 kA per cm of contact length and GaAs can carry 6.7 kA per cm of contact.⁴

An important consideration in dealing with high power, short-pulse lasers is the need for a very clean optical pulse. At some point in the lasing cycle a pulse is selected from a train of optical pulses. This invariably leads to a series of prepulses before the main optical pulse. Individually, these prepulses do not have sufficient energy to trigger the photoconductive switch. However, the long carrier recombination time in silicon integrates the energy of all the optical prepulses. The switch turns on with a slow ramp rather than an instantaneous transition. Even in GaAs, which has a rapid recombination time and is less likely to integrate the energy, the prepulses are quite damaging. The charge in the capacitive storage element will be diminished by the prepulses and the voltage switched to the load will be reduced. We used a series of Pockels cells (electronically controlled optical shutters) to produce laser pulse with a typical contrast ratio of 6000:1.

IMPROVED CONTACTS ON INTRINSIC SILICON FOR HIGH VOLTAGE PHOTOCONDUCTIVE SWITCHING

To construct a photoconductive switch, one must first deal with the problem of connecting the semiconductor to the external circuit. Thus, we must discuss fabrication of contacts on the semiconductor. When the silicon is subjected to extremely high electrical fields, a high dark current will begin to flow before the optical pulse arrives. This reduces the contrast between the on and off state of the switch. To obtain the highest resistivity possible, it is necessary to use very pure intrinsic silicon or highly compensated material. Any dopants normally added to commercial grade silicon will increase the conductivity. This leads to the problem of applying contacts to the intrinsic silicon. The semiconductor industry has studied numerous methods for placing contacts on silicon, but they normally work with extrinsic material and can vary the dopant levels under the contact to obtain ohmic contacts. Our objective was to present a method for placing ohmic contacts on intrinsic silicon without significantly increasing its conductivity. This problem has only recently received much attention.⁵ Most silicon photoconductive switches have operated

with only evaporated aluminum contacts.⁶ As we will report, Al contacts perform very poorly.

Initially we evaluated several methods for placing ohmic contacts on intrinsic silicon. All of the contacts were made by thermally evaporating either gold or aluminum on 1 mm thick wafers of intrinsic silicon over the entire wafer. The gold was 3000 Å thick and the aluminum was 9000 Å thick. The metallization layer was coated with photoresist and standard photolithographic techniques were used to make contact pads 1 mm x 2 mm with separation varying between 0.5 mm and 2 mm. The seven types of contacts which were applied to the silicon are listed in Table 1 below.

TABLE 1

Types of Contacts Applied to Silicon Switches

<u>Contact</u>
1. Evaporated Al no sintering
2. Evaporated Al sintered 1/2 hr 400°C
3. Evaporated Al through windows in an SiO ₂ passivation layer
4. Evaporated Al with n ⁺ doping under the metal layer
5. Evaporated Al followed by laser annealing the contact pad
6. Evaporated Au no sintering
7. Evaporated Au followed by laser annealing the contact pad

Each type of contact was tested to determine its I-V characteristic at voltages less than 400 V. This screening tests eliminated types 2, 3, and 4. All of these procedures involved the heating of the switch after aluminum had been applied. The result was that the resistivity of the bulk intrinsic silicon decreased. The decrease was so significant that the switches were inadequate for high power switching applications. The most likely

explanation for the reduction in resistivity was that impurities were diffusing into the bulk material. The obvious solution to this problem was to heat only the contact pads and not the bulk silicon. Laser annealing provides a means of localizing the heat applied to the silicon. Types 1 and 6 were mechanically unsound.

The initial work with the laser annealing was done with an amplified Q-switched, mode-locked Nd:YAG laser. A single 100 ps, 25 mJ laser pulse was focused on the entire 1 mm x 2 mm contact pad. The resultant switch had ohmic contacts but the system lacked reproducibility due to shot-to-shot laser fluctuations. An improved laser annealing system was developed in which a tightly focused laser beam was scanned across the contact pad. The laser spot size at the surface of the silicon was measured to be 100 μm . The energy in the pulse was 200 μJ to 400 μJ with a pulse duration of 100 ps. The laser system used to produce this pulse was described in the previous section. In the scanning mode, the spacing between the annealed spots could be varied, producing very uniform annealing at 25 μm separation or nonoverlapping spots at 100 μm separation as illustrated in Figure 2. The incident laser flux was typically 5 J/cm^2 . This is roughly twice the flux used in more conventional laser annealing of semi-conductor with cw or Q-switch lasers.⁷

Both types of laser annealed switches performed much better than any of the other types of switches. The first measurement made on the switches was the dc I-V characteristic. Figure 3 shows the I-V characteristic for a switch whose contacts were not laser annealed. The nonlinear relationship between the current and voltage shows that the contact is not ohmic. It behaves as diode rather than as a resistor. Figure 4 shows a switch whose contacts had been laser annealed. Between 0 V and 80 V the dc I-V characteristic is linear indicating an ohmic contact. The sharp break in the curve at 80 V is due to a change over from the ohmic to current injected regime. Below 80 V the current is carried predominantly by thermal electrons and holes generated in the semi-conductor. Above 80 V, the population of current carriers is determined by the free carriers injected into the semiconductor at the contacts. Although this looks like some sort of dielectric breakdown,

it is actually a well characterized phenomenon in solids. The current makes a discontinuous jump between a linear I-V characteristic and a V^2 current dependence.⁸

There are two major advantages to having good ohmic contacts on photoconductive switches. The contact is in series with the charge line so any resistance in the contact will present a discontinuity to the line which will generate reflections and lower the switch efficiency. A more damaging aspect of poor contacts comes from the electrical energy deposited in the contact. Any residual resistance in the contact will contribute to Joule heating of the switch. This may ultimately lead to switch failure. Therefore, lasers annealing of the contacts presents an easy methods of improving switch performance.

As mentioned earlier, silicon has a low resistivity. Therefore, it is impossible to place a high voltage dc bias across these switches.⁹ Thermal heating of the switch due to the dark leakage current leads to the generation of more thermal carriers. Eventually, thermal runaway will take place and the switch will start to conduct before it is triggered. For this reason the switches are normally operated in the pulse biased mode. A slow rising of a few microseconds duration is applied to the switch. The switch is triggered at the peak of the applied pulse to produce the jitter free, fast rise time electrical pulse.

The second phase of testing these switches was meant to simulate their operation in a pulse bias mode. The switches were mounted in a transmission line filled with silicone oil. This was necessary because the electrode spacing on the silicon was only 2 mm. Without the silicone oil the switches would have failed due to arching between the electrodes. With the oil present, it is possible to place 10 kV across a 1.5 mm gap without arching. The oil mounted switches were then pulse biased and the voltage and current were measured. A comparison between two switches is shown in Figure 5. The solid line indicates a switch with laser annealed contact pads and a 0.5 mm electrode separation. An identical switch, except that the contact pads were not laser annealed is illustrated by the dash line. The leakage current on the switch without processing was more than twice as large as that of the laser annealed switch. Thus, we have significantly improved the hold-

off characteristics of silicon photoconductive switches by laser annealing the contact pad. Similar results were obtained using a gold rather than aluminum as the metallization material.

Silicon photoconductive switches can be significantly improved by laser annealing the contact pads. When compared to the other types of contacts, the laser annealed contacts were ohmic and have a lower high voltage leakage current. Similar results have been seen with both aluminum and gold as the contact material. Although experiments are not in progress to quantify the difference, if any, between these two metals, the dominant factor appears to be the laser annealing. Very high laser intensities, due to the short duration of the laser pulse, are being used to produce these contacts. Some material is being ablated from the surface when the laser beam strikes. A possible explanation of what is happening is that the crystal structure of the silicon is significantly disturbed under the contact pads. A large number of trapping sites are introduced into the lattice which reduce the number of free carriers injected at the contact pads. With the injection current reduced, the switch behaves more like an open circuit. Koo *et al.*⁵ have found similar results by placing a layer of polycrystalline silicon underneath the contact pads. This amorphous layer reduced the injection of carriers into the switch. Laser annealing is a simple way to generate this same effect. The localized nature of the laser annealing means that we can alter the contact pads without affecting the bulk semiconductor material. This is very important because any change to the bulk material, such as introducing impurities by thermal diffusion, will adversely affect switch performance. The bulk material, where the electron hole pairs are generated by the laser trigger pulse, is not affected by the annealing. The switch efficiency as a function of the applied trigger pulse energy is the same for both the laser annealed switches and those that were not annealed at low voltage.

We discovered that thermal annealing of gold contact pads (450°C, 1/2 hr) did not cause the dc resistance of the switch to significantly decrease. Gold is a deep trap in silicon (i.e., it introduces trap states which sit in the middle of the forbidden band and are difficult

to ionize). Thus, even if gold was diffusing into the bulk, it would not interfere with the switch. Thus, there were three possible candidates for contacts to silicon:

1. Laser annealed Al
2. Laser annealed Au
3. Thermal annealed Au

The first two had reduced dark current leakage. The next test we performed were lifetime tests of the switches in actual operation. More than 10 million shot (1 kHz, 10 kV) in continuous operation could be obtained from the switches. However, the Al contacts were seen to degrade on the time scale of approximately two months. It was assumed that the Al was slowly diffusing. Of the two remaining contact types, both had advantages and disadvantages. The laser annealed Au seemed to have lower leakage but the thermal annealed Au had better current carry capability in the on state.

DIAGNOSTICS

There are no electronic probes that have picosecond time resolution and are capable of handling kilovolts. To determine if the switching is actually occurring on the picosecond time scale it is necessary to use fast optical probes to characterize the circuits. An electro-optic crystal placed in an electric field experiences a change in its birefringence. This effect can be viewed as the mixing of a dc electric field and an optical field in a crystal to produce a new optical field with its polarization rotated with respect to the original optical field. The change in the birefringence is monitored by probing the crystal with polarized light as shown in Fig. 6. The light passes through a polarizer; a compensator, to provide an adjustable bias to the transmission; the electro-optic crystal; and the reflects off a dielectric mirror to retrace its path or continue on to a second crossed polarizer in transmission mode. In reflection mode, the polarizer is effectively crossed with respect to itself because of compensator. When the crystal is placed between crossed polarizers, the transmission is given by:

$$T = \sin^2\{[(KEl_c) + \phi]/2\} \quad (1)$$

where E is the magnitude of the low frequency electric field; l_c is the optical path length through the crystal; ϕ is a constant optical rotation due to the compensator and static birefringence of the crystal; and K is a constant that depends on material parameters, the crystal orientation and the frequency of the optical field.¹⁰ By choosing the type of crystal and its orientation, the Pockels effect can be made sensitive to only one spatial component of the applied electric field. We have used this technique in a number of different circuits. In a coaxial line a LiTaO_3 crystal orientated with the optic axis along the radius selected only the radial field. A radial transmission line was investigated by placing a KDP crystal between the plates at the center with the z axis normal to the plates to measure the field between the plates. The configuration shown in Fig. 6 was used for planar circuits. In all instances, a fraction of the IR pulse used to trigger the switch was split off, frequency doubled, and used to probe the electro-optic crystal. The component of the electric field, orthogonal to the original polarization direction, was rejected by the polarizer and detected by a photodiode. The compensator was set so that after the double traverse, the light was circularly polarized and the light at the detector was biased to half of maximum intensity, thus, the optical probing system. A variable delay line in the one of the optical beam lines provided the temporal scanning. As the length of the delay line increased the modulation of the optical beam changed and the electrical pulse shape was mapped out.

FIELD DEPENDANCE OF THE RISE TIME

Experiments in the coaxial geometry indicate that the rise time of the electrical pulse is a function the applied optical energy and the electric field. A small piece of LiTaO_3 was placed in the line 5 mm from the switch and was probed with the second harmonic of the trigger pulse. The optical energy was varied by using a half wave plate and a polarizer. Figures 7 and 8 show the results at two different voltages. For both voltages, the rise time increased as the optical energy increased. The peak electrical pulse occurred at later times

with respect to the optical pulse as the optical energy decreased. The differences between the two voltages is very interesting. Although the optical energies are the same for each family of curves, the rise time is significantly longer as the voltage was reduced for corresponding optical energies. If the electrical state of the switch was determined by only the integral of the absorbed optical energy, the shape of the electrical pulses should be independent of the voltage. Something more complicated happens than the simple addition of carriers.

The current density in the switch is given by: $j = nev$ where n is the carrier density, e is the electronic charge, and v is the carrier velocity. However, in the highly stressed regime that we operate, the velocity of the carriers in silicon is saturated and the velocity versus field curve is nonlinear. Figure 9 illustrates this nonlinearity. At different voltages, the switches have an initial state at different points along this curve. After enough carriers have been generated, the field collapses to the linear regime. But at each voltage the system will follow a different path to that final state. Thus, the rise time of the switch was determined to be field dependent.

Picosecond high voltage switching requires the combination of high-energy, short-pulse lasers, large bandwidth electrical geometries, large voltage standoffs and gigahertz diagnostics. However for specific applications such as short-pulse, high-gradient electron accelerators it is the only method available. As we have seen with the coaxial lines, careful control of the light intensity and field is necessary to achieve the desired rise time.

CARRIER LIFETIME MEASUREMENT

The switching efficiency was characterized to determine the optimum optical intensity needed to drive these switches. In the lifetime tests described earlier the switches were driven with 300 μ J of optical energy. This was more than sufficient to drive the switch into saturation and laser power was not the limiting factor. In applications, the laser power becomes a constraint. The lowest light level that could be used to fire a switch

described above and still keep the switched voltage within 10% of its saturation level was 70 μJ in a Gaussian spatial profile. To get the fastest possible rise time, it was necessary to have the most uniform possible illumination of the switch. Unfortunately the circular profile did not match the 2 x 2 mm² rectangular switch cross section. The best results in terms of switching were obtained with a spot size chosen to have its $1/e^2$ diameter 20% greater than the separation between the electrodes. With this intensity, the normalized switched waveform remained unchanged over the range of 100 V to 10000 V. This established the lower bound on the optical energy.

The upper bound of the optical energy was established by the carrier concentration. If too many carriers were generated in the semiconductor, the carrier lifetime became dominated by Auger recombination. The carrier density began to fall off very rapidly with increasing carrier density. This resulted in the switch shutting off prematurely. The normal carrier lifetime was measured by activating the switches with an optical pulse without having a voltage applied. The electrical conductivity was then probed with a short electrical pulse at a later time. This experiment demonstrated that the normal carrier lifetime in these samples was about 70 μs . However, there also appeared to be a fast component associated with this decay. To study this component a 100 ns charge line was attached to a photoconductive switch and various optical intensities were applied to the switch under bias. Normally, the switched waveform would be a square pulse with a duration equal to twice the electrical transit time of the charge line. The fast component of the carrier recombination time manifested itself as a drooping of the top of this square pulse as illustrated in Fig. 10. This drooping was modeled with a decaying exponential. The lifetime associated with this exponential is plotted versus the initial concentration of carriers in Fig. 11. Below 10^{17} cm^{-3} the apparent lifetime increases with increasing carrier concentration. This may be associated with some form of carrier sweep out. Inducing more carriers compensates for the lost carriers and results in a longer effective life time. As the concentration increases even further the lifetime starts to decrease again. This is

probably due to Auger recombination. A rapid processes involving a three-body collision of carriers in the semiconductor that becomes significant at high densities.

TEMPERATURE PROBING

The operational parameters of these switches have also been investigated. A technique has been developed to measure the temperature of a silicon photoconductive switch while in operation. At a wavelength of approximately $1\ \mu\text{m}$ the optical absorption of silicon is a very sensitive function of temperature. Silicon is an indirect bandgap material and has a band edge that extends over a large spectral region.¹¹ As the temperature changes, a fixed optical wavelength will sample different points along the transmission curve. Some of the 1.06 mm light used to trigger the switch leaks through and it is this light that is detected to measure the temperature. The 200 μm and 500 μm thick switches used in this experiment allowed a few percent of the incident light to leak through. The optical transmission was found to be a function of the voltage applied to the switch. Figure 12 shows change in temperature as monitored by the optical transmission in a silicon photoconductive switch biased at 300 V. The switch was triggered at 1 kHz. The temperature measurement was calibrated by first placing the switch in an oven and measuring the transmission as a function of temperature. The relatively long response time of 10 seconds indicates that a thermal process was responsible for the change in optical transmission. The optical pulse was present before and after the voltage was turned on, thus eliminating the possibility that the heating of the switch was due to adsorption of the optical pulse. The most probable cause was the heating of the switch by the electrical current.

The transmission line connected to the switch for this experiment was charged with a pulse that was long with respect recombination time of the carriers in silicon. Thus the trailing edge of the electrical pulse was determined by the trailing edge of the charging pulse and the carrier recombination time. The switch continued to conduct for a long time with a

resistance that increased exponentially with the recombination time. Most of the heating of the switch occurred during this transition time. The heating of the switch could be significantly reduced even at much higher voltages by using a bias pulse much shorter than the recombination time, thus turning the switch off faster. This highlights the need to have rapid turn on and turn off times in pulse power applications.

SURFACE FIELD

The driving force behind this portion investigation was the need to understand surface breakdown on semiconductors. Many applications require that electrodes on semiconductor materials be placed in geometries where significant electric fields are developed across their surfaces. This generalization is true over a wide range of applications. High-speed semiconductor circuits such as those in VLSI applications, place relatively small voltages across the electrodes, but the electrode separation is made as small as possible to reduce the signal propagation time through the device. This results in large electric fields. Pulsed power semiconductor switches have relatively large electrode separations, but they are required to hold off very large voltages. Surface breakdown is the major limiting factor in the operation of these elements. Whether the circuits are for high speed logic or pulse power, the need to keep the surface electric fields below the level where surface breakdown will occur places a minimum size restriction on the devices that can be constructed. Despite its relevance, the mechanism of surface breakdown on most materials is poorly understood. Semiconductors, in particular, are difficult to understand because of the presence of free carriers on the surface which modify the distribution of the electric field. This section presents the development of an imaging technique to monitor the temporal evolution of surface electric fields. These experiments seek to use this information to reconstruct the dynamics of the charge carriers on the semiconductor surface.

To measure the surface electric fields we used the Pockels effect described earlier. It can modulate an optical probe to produce an optical replica of the electric field under investigation. The response time of the electro-optic material is of the order of femtoseconds, which allows for extremely high bandwidth signal acquisition. The unique features of electro-optic sampling are its speed and noninvasive nature. Electro-optic sampling techniques have measured electrical rise times as short as 300 fs without loading the circuit.¹² Because the probe is optical, no electrical contacts, which can perturb the device under test, are needed. The optical coupling also means that the detection electronics are isolated from any dangerous high voltage transients at the test circuit. By choosing the type of crystal and its orientation, the Pockels effect can be made sensitive to only one spatial component of the applied electric field, as shown in Fig. 13.

The dielectric mirror is bonded directly to the electro-optic crystal and the entire assembly is placed directly on top of the surface to be monitored. The surface to be monitored had two rectangular electrodes separated by a fixed distance. The crystal used in these experiments was LiTaO_3 . Its optic axis was perpendicular both to the direction of light propagation and the edges of the electrodes. Thus the optic axis was orientated along the electric field lines and the Pockels effect was sensitive to only the component of the electric field along that axis.

The principle assumption of this work was that the measured electric field was not uniform over the surface being measured. Two configurations were used to detect the spatial and temporal variation of the electric field. The initial measurements investigated the low voltage quasi-static configuration of the surface electric field. A piece of LiTaO_3 was placed across evaporated metal contacts on both silicon and gallium arsenide. A time varying potential was induced across the contacts. This induced a modulation of the birefringence of the LiTaO_3 in both space and time via the Pockels effect. A tightly focused cw HeNe laser, with a spot size of approximately $40 \mu\text{m}$, probed the change in birefringence. The spatial profile was obtained by translating the electro-optic crystal and

semiconductor such that different points were illuminated by the laser beam. The low voltage applied to these devices produced very weak modulation of the the optical signal requiring that the signal be extracted with phase sensitive detection. This experiment demonstrated that we could spatially resolve the surface electric field on the surface of the semiconductor.

The data acquired as described above had two serious drawbacks. It lacked temporal resolution and required that the beam be scanned spatially to acquire the total spatial variation of the field. Such conditions are incompatible with the need to record spatially nonlocal, transient events typical of a surface breakdown. The second phase of our investigation addressed these issues.

Short pulse laser probes improve the time resolution. A single light pulse from a frequency-doubled, mode-locked, amplified Nd:YAG laser samples the electric field only while it traverses the sampling crystal (~100 ps). This technique works with a single optical pulse only at field strengths that are comparable with the field necessary to cause the the direction of the polarization vector in the sampling crystal to change by one half wave (~1-10 kV/mm). Otherwise the optical modulation would be too weak to be extracted without the aid of extensive signal processing. The study of surface breakdown events, where the sample may be damaged on a single shot, requires unambiguous single shot detection. With short pulse lasers, it is possible to take 100 ps snapshots of any given event. A series of snapshots of the surface electric field can be taken to record the temporal variation in the field.

The spatial variation in the surface field can be monitored by illuminating the entire area of interest. Instead of using a single detector and scanning a tightly focused spot, a detector array captures an image of the entire field of interest. Each detector element measures only a small portion of the electric field. This experiment has been carried out using an 512 element linear intensified diode array. A 2 mm gap with identically prepared gold-coated, laser-annealed contacts on intrinsic silicon (7000 Ω cm) was pulsed biased

with a short electrical pulse synchronized with respect to the laser pulse. A 50Ω load was placed on the low side of the silicon and the leakage through the material was monitored. The lack of photoconductive switching at the load guaranteed that none of the light coupled through the dielectric mirror into the silicon. It is important that light does not perturb the field. During the actual acquisition of data, the load was attached directly to ground. The laser illuminated a circular region on the silicon surface. The detector acquired a one-dimensional slice of the electric field on a line joining the two electrodes midway between the ends of the electrodes. This is the first demonstration of imaging technology applied to electro-optic field measurements.

The electric field distribution produced by the electrode distribution used in these experiments is not uniform. It is a common field configuration encountered when fabricating devices on wafers (e.g. coplanar transmission lines between transistors in VLSI circuits or photoconductive switches fabricated on wafer substrates). The fields lines in a plane perpendicular to the surface are shown in Fig. 14(b). They may be derived from the simple case illustrated in Fig. 14(a) by the operation of the conformal transformation:¹³

$$z = 2 \ell_n \left\{ [1 + \sin(w)]^{1/2} + [b_z + \sin(w)]^{1/2} / (b_z - 1)^{1/2} \right\} \quad (2)$$

Followed by the second transformation:

$$z' = w_d - 2 \ell_n \left\{ \frac{[1 + \sin(iz + \frac{\pi}{2} - iw_g)]^{1/2} + [b_z + \sin(iz + \frac{\pi}{2} - iw_g)]^{1/2}}{(b_z - 1)^{1/2}} \right\}, \quad (3)$$

where

$$b_z = 2 \coth^2(\pi \ell_c / 2 \ell_s) - 1 \cong 1, \quad (4)$$

w_g is the normalized gap width, l_c is the electrode length, and l_s the substrate thickness, $w = u + iv$, $z = x + iy$.

These transformations fold the electrode end faces out into the coplanar geometry. The second transformation is only valid if the transformed plane is at infinite distance from the first plane because the electric field lines must be normal to the second plane. However, if the electrodes are sufficiently far apart, the deviation from normal incidence is negligible. These transformations define the expected value of the electric field throughout the volume of the semiconductor provided that the measurement is not taken near the corners of the electrodes. The fringing field outside of the semiconductor can be inferred from electro-magnetic theory (i.e., the tangential component of the electric field is continuous across a dielectric interface).

From the known electric field configurations in Fig. 14(a), the electric field in Fig. 14(b) can be calculated. For the type of electro-optic crystal that was used in this experiment, the electric field along the x' axis in Fig. 14(b) was measured. Figure 15 shows the field in the plane of the interface. The features are exactly as expected. Above the contacts the electric field is normal to the surface. Therefore, the field along the x' axis is zero. At the edge of the contacts the field lines bunch-up due to the attraction of charges on the opposing electrodes. However, this is not what is actually measured. What is actually measured is the phase shift:

$$\theta = \int_{IA} dA \int_0^L KE_x(x,y) dx. \quad (5)$$

This integral is over the thickness of the electro-optic crystal (L) and is clearly dependent on that thickness. Figure 16 shows the integrated detected signal as a function of the electro-optic crystal thickness. The uppermost curve indicates what happens if the crystal is so thick that the integral extends over all the field lines. The surface features are

completely obscured because the total integrated flux is conserved between the electrodes. Alternatively, if the crystal is too thin, then the modulation imparted to the light signal becomes very small. The amount of rotation is proportional to the optical path-length in the crystal. An intermediate thickness ($\sim 1/4$ to $1/5$ of the distance between the electrodes) must be chosen that balances the magnitude of the extracted signal with the smearing due to the path length integration. Additional smearing of the detected signal, due to the finite size of the sampling beam, is also incorporated into the calculation of the curves in Fig. 16. The signal must be averaged over either the laser spot size or the size of the detector element on which it is imaged. In Eq. (5) this is represented by the integral over the illuminated area (IA).

The usefulness of this technique has been demonstrated at low voltage where the preparation of the contacts on the semiconductor has been shown to influence the dc electric field distribution. This is the work that was done with the cw probe and the phase sensitive detection. The primary purpose of the cw experiments was to demonstrate that we could detect spatial variations in the field. The electric field was essentially dc (actually a low frequency, 1 kHz, square wave). In addition to demonstrating the ability to monitor surface fields, these measurements proved a reliable method of characterizing the contacts. Figure 17 shows a cross-sectional view of the field along the center line between the contact pad on GaAs. The figure shows the general features that are expected; the bunching at the contacts and the tailing off at the electrodes. The sampling crystal was thick with respect to the to the electrode separation. Therefore, the peaks exhibit a significant amount of smearing. What is most interesting is the asymmetry of the electric field. The contacts were identically prepared. So no asymmetry was expected from the material properties of the sample. When the polarity of the applied bias was reversed, the asymmetric field distribution also reversed. This indicated the contacts were not ohmic with respect to the different carrier species (electrons and holes).

The cw data also showed that a full two-dimensional map of the electric field could be acquired. Figure 18 consists of axonometric plots of the electro-optic image of the electric field on a GaAs switch for different probe crystal thicknesses. The electric field tails off as the probe moves away from the center line of the electrodes.

The time resolved data was taken to determine the time scale on which the asymmetry illustrated in the cw data evolved. The data was taken by grounding one of the electrodes on a sample prepared on high resistivity silicon ($\rho = 7 \text{ k}\Omega \text{ cm} = 70 \text{ }\Omega\text{m}$). The dielectric relaxation time of this material is given by the product, $\rho\epsilon = (70 \text{ }\Omega\text{m} \times 11.9 \times 8.85 \times 10^{-12} \text{ F/m})$. Where ϵ is the dielectric constant of the silicon. Thus on time scales less than 7 ns, silicon will have a transient response to an applied electric field. A photoconductive switch was used to pulse bias the test structure on a time scale less than 200 ps. One electrode was grounded and the other was attached to a terminated 50 Ω line driven by photoconductive switch. The switch was triggered with a 1.06 μm light pulse from a Nd:YAG regenerative amplifier. A 0.532 μm pulse, derived by frequency doubling a portion the 1.06 μm light, probed the LiTaO_3 crystal. An optical delay line in the path of the 1.06 μm light provided a variable time delay in the between the voltage and probe.

The optical image of the electric field was measured with a gated diode array at various time delays between the pump and probe. Figure 19 shows three traces of the surface electric field of a device with a 2 mm gap pulsed with 1 kV at various time delays. The units of vertical axis are in percent modulation of the light signal. This is the signal obtained with the voltage on; minus the signal with the voltage off divided by the signal with the voltage off. Thus the detected modulation was relatively immune to variations in the illumination profile. At very early times (A), very little voltage has built up but the device appears to be symmetric in response to the electric field. Curve (B), 166 ps later, shows that a significant voltage has built up across the device and the field is still symmetric. At 332 ps after (A), curve (C), the voltage is still rising but the field shows a definite asymmetry.

The simple explanation of this data is that at early times the electrical inertia of the silicon prevents it from reacting to the field. The device then behaves as if it were a perfect dielectric. The field rises symmetrically on both electrodes and is determined only by the electrode configuration. Later, as the charge carriers in the silicon begin to rearrange in response to the field, the field itself is modified by the charges in the silicon. Thus, the asymmetry seen in the cw data begins to manifest itself on the time scale of a few hundred picoseconds. This shows that it is possible to probe the transient response of a semiconductor which has been biased on a time scale that is short compared to the dielectric response time of the material.

Although the applied fields were less than those necessary to cause breakdown, some features about the semiconductors could readily be discerned from the electro-optic imaging data. In the dc biasing case, the contacts were asymmetric with respect to the applied voltage. One contact always had a higher field enhancement at the edge than the other. The enhancement shifted as the polarity of the applied voltage reversed. Such field enhancements are probably due to differences in the injection of holes and electrons at the contacts. They may play an important part in initiating breakdown. The pulse bias case illustrated that this data could be taken on a very short time scale and transient structure of the electric field can be observed. By probing at different times and places we can produce a two-dimensional map of the time evolution of the electric field on a semiconductor surface.

RADIAL LINE

In addition to looking at the operation of photoconductive switches, we looked at some novel switch geometries. One such geometry is illustrated in Fig. 20. This structure can be used to build a compact electron accelerator. A radial transmission line is connected to a high voltage feed (DC or quasi-DC) through a piece of semi-insulating material such as chromium doped gallium arsenide (Cr:GaAs) or Si. When the

semiconductor is illuminated with an optical pulse, charge is transferred to the metal disks and a pulse propagates inward toward the hole in the center of the disks where the electrons will pass through the structure. The characteristic impedance of the line at radius r and plate separation d is given by:¹⁴

$$Z(r) = (d/2\pi r)(\mu/\epsilon)^{1/2} \quad (6)$$

at moderate values of the radius. For very small values of the radius the impedance is given by:

$$Z(r) = -j (\mu/\epsilon) [(kd/2\pi) \ln(kr)] \quad (7)$$

where:

$$k^2 = \mu\epsilon\omega^2$$

and ω is the electrical frequency.

The voltage squared is proportional to the impedance. The pulse does not significantly broaden as it propagates, so the power (proportional to V^2) is constant. Therefore, the voltage gain will go as $(r_i/r_f)^{1/2}$, where r_i is the initial radius and r_f is the final radius, provided that the final radius of the center hole is not too small. The dimensions of a structure that is under consideration are: a plate separation of 1 mm; an outer radius of 30 mm; and a hole radius of 0.5 mm. The ratio of the radii suggests an estimate of ten for the voltage gain. A numerical model employing a finite difference solution to Laplace's equation in cylindrical coordinates indicates a possible electric field gain of 12.5 for a 8 ps optical pulse. The results of that calculation are shown Fig. 21.

The plate separation distance determines the impedance of the transmission line. However, because of the finite transit time of electrons between the disks, the gap also determines the energy delivered to the electrons by a finite duration electrical pulse. The numerical results for the effective electric field seen by an electron passing through a field with finite rise time can be approximately summarized by:¹⁵

$$E_c = 2E_0(2r_i/g+c\tau)^{1/2} \quad (8)$$

where E_c is the effective electric field at the center of the disks; E_0 is the electric field at radius r_i and τ_r is the rise time of the pulse; and g is the gap between disks. Equation (8) shows the importance of ultrafast switching in maintaining a small gap between the disks.

If the photoconductive switch is pulsed biased, it should be possible to place 40 kV across the switch without breakdown. This is not unreasonable because Si has withstood 100 kV/cm in a 3 μ s pulse.¹⁶ When this 40 kV pulse propagates to the center of the disk, the electric field will be amplified to 400 kV/mm or 0.4 GeV/m. This field would cause problems in a conventional RF linac; however for a switched power linac described above the simulation shows that the electric field drops by a factor of 2 in 10 ps and a factor of 5 in 60 ps. Thus it is very unlikely that breakdown will occur.

The trade-off for such a high gradient is a very short time window in which the electrons may be accelerated. This system cannot tolerate any jitter between the electrical pulse and the optical pulse or between the electrical pulses on successive stages. Fortunately, optical activation of the switches is inherently jitter-free. The only mechanism controlling the switching is the absorption of light. If the thickness of the switch is well matched to the absorption depth of the light, the carriers will be generated uniformly throughout the bulk of the device. Thus, if the energy of a single optical pulse is distributed into a number of synchronized optical pulses, the electrical switches activated by those smaller pulses will be exactly synchronized. The synchronization between the electrons and the acceleration gradient is easily accomplished by generating the electron pulse photoelectrically with a small portion of the optical pulse.

The structure used in this investigation is shown in Fig. 20. The lower brass disk is grounded and the upper disk is a silicon wafer 500 μ m thick. The initial structure was smaller than we eventually intend to use but we were still able to measure gain. A gold coating on the inner side of the silicon served as the "anode" to provide the conducting structure in which the pulse propagates. A ring of gold coating, connected to the high voltage feed, was deposited on the other side of the silicon at its outer circumference. The

two disks were separated by 2 mm and had a 1-mm diameter hole at their center. A circular 2-mm-thick KDP crystal was placed at the center; it was 7 mm in diameter and had a reflective coating on one side. A hard tube pulser provided the high voltage that was applied on the outer diameter of the disks 10 ns – 100 ns before switching. The equivalent electric circuit is shown in Fig. 22. The disk structure is represented by C2, even though at these speeds it is a distributed system; C1 is the charging capacity; C1 ~20 pF; and R1 represents the ohmic impedance across the silicon disk between the conducting coatings R1 ~10 K Ω ($\rho = 7$ k Ω -cm). S2 represents the photoconductive switch, which shorts R1. When the charging pulse V_0 is applied at C1, the upper plate of C2 floats towards V_0 , charging up C2; to prevent this, a small conducting spring, indicated by the inductance L1, was inserted between the disks. The inductance should be an open circuit at the high frequencies propagating on the disk, but it is a short circuit to the unwanted low frequencies. The waveform at the charging electrode (i.e., the C1, R1 node) is shown in Fig. 23(a). Because of the impedance mismatch, the voltage builds up to V_0 by successive reflections; the IR switching beam is blocked. Figure 23(b) shows the waveform when switching takes place by the IR pulse, whose timing is indicated on the lower trace. The outside ring can be completely shorted to the inner disk.

The electrical signal at the center was mapped out by introducing a variable delay between the infrared and visible pulses. To improve signal to noise, the electrical pulse was applied on every second laser pulse and the difference between 20 consecutive pulses was averaged in a boxcar integrator. Furthermore, the incident-pulse intensity was monitored and used for normalization. The crystal was calibrated by applying a (quasi) static voltage (1.5 kV) across the disks. The results of the calibration are shown in Fig. 24 and correspond to an optical bias of the compensator plate of $\phi = 0^\circ$, 45° , and 90° , respectively. At 45° , the rotation induced by the voltage pulse, which is applied for every second laser pulse, is clearly shown as a distinct trace. At 0° and 90° , the signal is quadratic in the optical rotation angle and beyond our resolution. The optical delay line had

a travel of 9.4 cm and a step size of 6.25 μm . Data points were taken every 25 steps or 1.04 ps. However, the time resolution of the system is set by the thickness of the crystal. Since the probe beam traverses the 2-mm-thick crystal twice (given a refractive index $n = 1.5$) the optical pulse is subject to the influence of the electrical field for 18 ps.

The best waveform observed is shown in Fig. 25. The measured rise time (10% to 90%) is $t_M = 24$ ps; this is a convolution of the actual rise time with the time resolution of the probe, 18 ps. By simple quadrature, the true rise time is $t_R = 16$ ps. In addition, the effect of the KDP crystal must be considered. The effective dielectric constant is approximately 20.¹⁹ This will result in only 37% of the energy being coupled into central portion of the disk. Thus the measured gain must be further multiplied by a factor of 2.27. A reflected pulse appears ~ 300 ps after the initial pulse. This corresponds roughly to the transit time for the round trip from the center of the disk to the edge of the structure and back (8 cm). Based on the calibration of the crystal, the observed peak field is $V_c = 1.0$ kV. The charging voltage was $V_o = 480$ V, so that the observed gain is $V_c/V_o = 2.08$. This can be compared with the analytic formula Eq. (8). Even though Eq. (8) is the energy imparted to a relativistic electron traversing the gap, it still bears some applicability to this experiment. Equation (8) takes the quantity $E(t) \cdot \Delta g$ [where $E(t)$ is the time varying electric field in the gap and Δg is an incremental distance in the gap] and integrates that quantity over the time that the electron is in the gap. This experiment injects a light pulse into the gap that experiences a rotation of its polarization proportional to $E(t) \cdot \Delta g$. Thus the two different probes (the photon and electron) measure the same quantity. The gap must be doubled to account for the double traversal of the light, and the speed of light must be divided by $20^{1/2}$ to account for the reduced speed of propagation of the electrical signal in the KDP. To predict the gain from Eq. (8), we use $t_R = 16$ ps, $R = 3$ cm, and $g/2 = 0.2$ cm. The calculated gain is then 5.82. If the measured gain of 2.08 is multiplied by 2.27, we obtain 4.73 ± 0.44 , which is somewhat less than predicted. The

discrepancy is probably due to finite size of our sampling beam which illuminated regions of lower gain.

Thus, we have shown that photoconductive switches can be used to activate a switch in a radial transmission line geometry. The structure investigated, has demonstrated gain in approximate agreement with theoretical predictions and the device may be useful as an accelerating element in a compact electron accelerator.

SUPERCONDUCTING OPENING SWITCHES

During the past year, we have looked at other optically activated switches. Specifically, we have looked at the possibility of making an opening or photoresistive switch by illuminating a superconductor with a laser. We are happy to report that we have managed to operate such a switch at low power.

The switch was fabricated from a thin film of yttrium barium copper oxide (YBCO). The film was deposited on a yttria stabilized cubic zirconia (ZrO_2) substrate and was 1.3 μm thick. The thin film was fabricated by Dr. Alan Kadin's research group in the Electrical Engineering at the University of Rochester. The switch was constructed by using the 1 kHz regenerative amplifier described earlier to pattern an "H" on the film. The laser was focused to a 6 μm spot size on the film to locally ablate the superconducting material without affecting the adjacent material. The resistance verses temperature curve for one of these switches is shown in Fig. 26. The cross bar of the "H" (which actually constituted the switch) was 0.2625 mm x 2.5 mm.

The "H" pattern was a convenient structure for testing for an opening switch. A Thevenin equivalent circuit ($V_{th} = 1.25$ V, $R_{th} = 1.13$ K Ω) was attached across the upper two arms of the "H". The output voltage was measured across the lower two arms of the "H". A model of this circuit is shown in Fig. 27. When the sample is superconducting, the crossbar of the "H" shorts out the load. When the sample is in the

normal state, a voltage will appear across the output because the output will no longer be shorted to ground by the superconductor.

From Fig. 26, we can see that if the laser pulse drives the sample to room temperature, the resistance will increase from 0 to about 150 Ω . The superconducting film used in these experiments had a resistivity 10 Ω /square. Although the film could be made more resistive in the normal state by altering the deposition processes, this is not desirable. It is a general rule of thumb that films with high room temperature resistivity have a low transition temperature and a depressed critical current. Higher resistances are best obtained by altering the geometric aspect ratio of the superconducting switch.

The sample was illuminated with 1.06 μm radiation. The laser intensity was between 1.5 and 5.5 mJ/cm^2 in a 200 ps pulse at 53 Hz. Figure 28 shows the voltage measured at the load for one particular intensity. The initial temperature of the switch was just below the transition temperature (76 $^\circ\text{K}$). The magnitude of the load voltage indicates that the final resistance was 71 Ω . The rise time of the switch appears to be due to the RC time constant of the load capacitance which was introduced by the cables coupling the signal out of the cryostat. However, this question is still unresolved. From the measured optical absorption coefficient, $8.4 \times 10^4/\text{cm}$, we calculated an instantaneous temperature distribution as shown in Fig. 29. Using values for the heat capacity and thermal conductivity obtained from the literature,¹⁷ we can show that the absorbed optical energy has not reached the rear surface of the YBCO in 50 ns. Thus, part of the rise time may be due to the thermal effects in the sample. The final voltage measured at the load, indicated that the sample had achieved a final temperature of $\sim 100^\circ\text{K}$. This is less than would be expected if the sample were uniformly heated by the laser pulse but more than would be expected if the resistance was calculated by integrating over the temperature profile. We were operating near the critical current, $\sim 10^2 \text{A}/\text{cm}^2$, and assumed that since YBCO is a type II superconductor, normal and superconducting regions could exist simultaneously. One

explanation for these results may be that the electrons were being heated independent of the lattice, i.e., Cooper pairs were being broken.

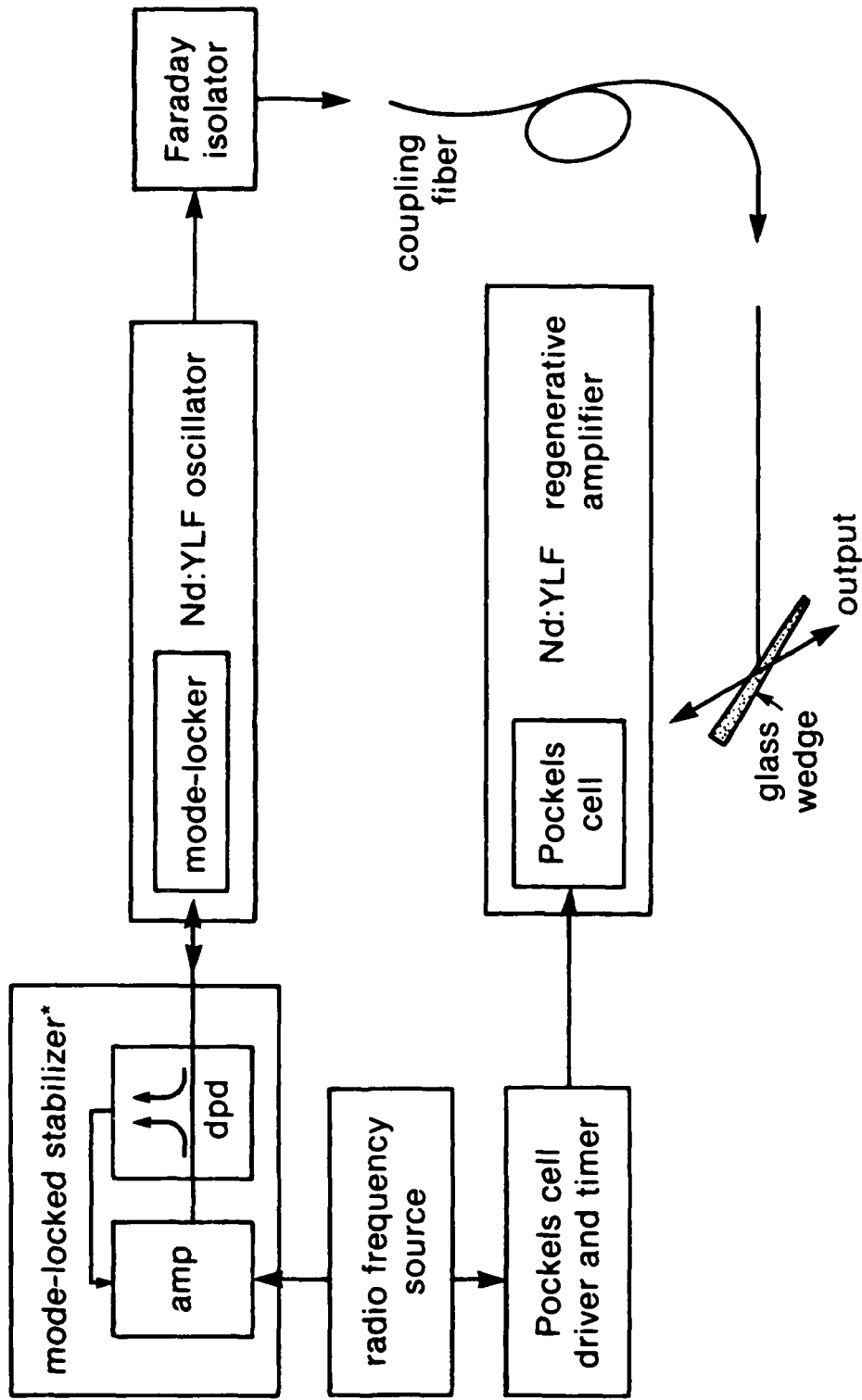
In any event, we have shown that repetitive opening switches can be constructed from optically activated ceramic superconductors. With improved materials, $J_{\text{critical}} > 10^5$ and larger switches, we should be able to scale to higher powers.

REFERENCES

1. G. Mourou, W. H. Knox, and S. Williamson, "Picosecond Switching in Semiconductors" Picosecond Optoelectronic Devices, edited by Chi H. Lee (Academic Press, New York, 1984), pp. 219–248.
2. A. Antonetti, M. M. Mally, G. Mourou, and A. Orszag, "High Power Switching with Picosecond Precision: Applications to High Speed Kerr Cell and Pockels Cell," Opt. Commun. **23**, pp. 435–439 (1977).
3. D. Strickland, and G. Mourou, "Compression of Amplified Chirped Optical Pulses," Opt. Commun. **55**, 447–449 (1985).
4. W. C. Nunnally and R. B. Hammond, "Optoelectronic Switch for Pulsed Power," Picosecond Optoelectronic Devices, edited by Chi H. Lee (Academic Press, New York, 1984), p. 509.
5. J. C. Koo, G. M. McWright, M. D. Pocha, and R. B. Wilcox, "A Low Leakage 10000V Silicon Photoconductive Switch," Appl. Phys. Lett. **45**, 1130–1131 (1984).
6. W. C. Nunnally and R. B. Hammond, "80-MW Photoconductor Power Switch," Appl. Phys. Lett. **44**, 980–982 (1984).
7. P. Baeri and S. U. Campisano, "Heat Flow Calculations," in Laser Annealing of Semiconductors, edited by J. M. Poate and J. W. Mayer (Academic Press, New York, 1983), pp. 75–109.

8. M. A. Lampert and P. Mark, Current Injection in Solids (Academic Press, New York, 1970), Chapter 2.
9. G. Mourou and W. Knox, "High-Power Switching with Picosecond Precision," Appl. Phys. Lett. **35**, 492-495 (1979).
10. A. Yariv, Quantum Electron., 2nd ed. (John Wiley & Sons, New York, 1975), p. 407.
11. S. M. Sze, Physics of Semiconductor Devices 2nd ed. (John Wiley & Sons, New York, 1981).
12. J. A. Valdmanis, G. A. Mourou, and C. W. Gabel, "Picosecond Electro-Optic Sampling System," Appl. Phys. Lett. **41**, 211-212 (1982).
13. P. M. Hall, "Resistance Calculations for Thin Film Pattern," Thin Solid Films **1**, 277-295 (1967).
14. K. Mittag, A. Brandelik, "Matching Problems in Pulse Power Radial Transmission Lines," in Digest of Technical Papers, Fifth IEEE International Pulsed Power Conference, edited by M. F. Rose and P. J. Turchi (IEEE, Piscataway, NJ, 1985), p. 511.
15. R. E. Cassell and F. Villa, "Study of a high gradient pulsed linac structure," SLAC-PUB-3804 (October 1985). Also F. Villa, "High gradient Linac prototype: A modest proposal," SLAC-PUB-3875 (January 1986).
16. J. T. Milek and M. Neuberger, Linear Electrooptic Modular Materials (IFI/Plenum, New York, 1972), p. 177-222.
17. C. Zhaojia, Z. Yong, Y. Hongshun, C. Zuyao, Z. Dongnin, Q. Yitia, W. Baimei, Z. Qirui, Solid State Commun. **64**, 685-687 (1987).

Nd:YLF Mode-Locked Oscillator and Regenerative Amplifier

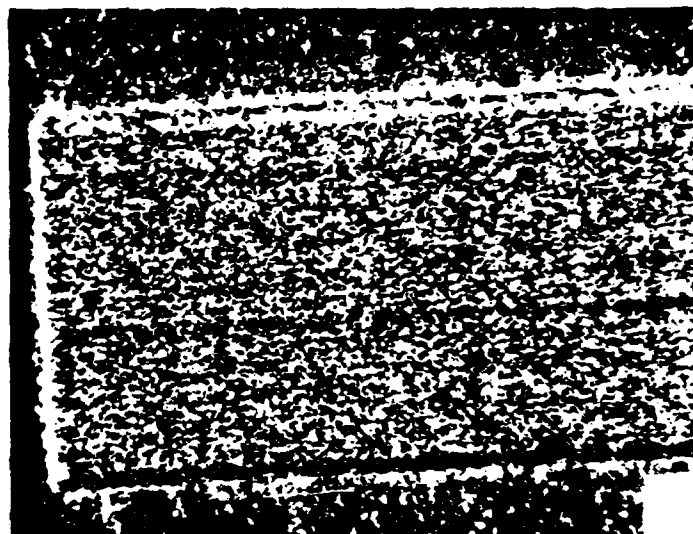


*H. Klann et al., *Optics Commun.* **38**, 390 (1981).

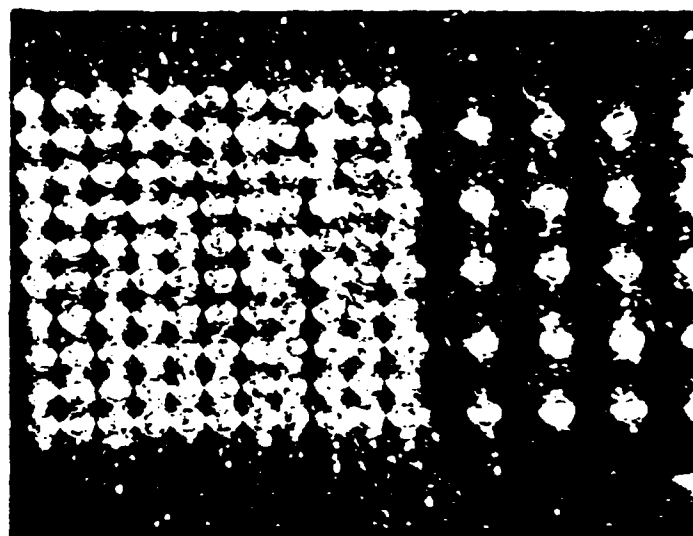
Fig. 1

Optical Micrographs Showing the Effects of Laser Annealing of 3000-Å Au Film on Si

UR
LLE 



25- μm
spot separation



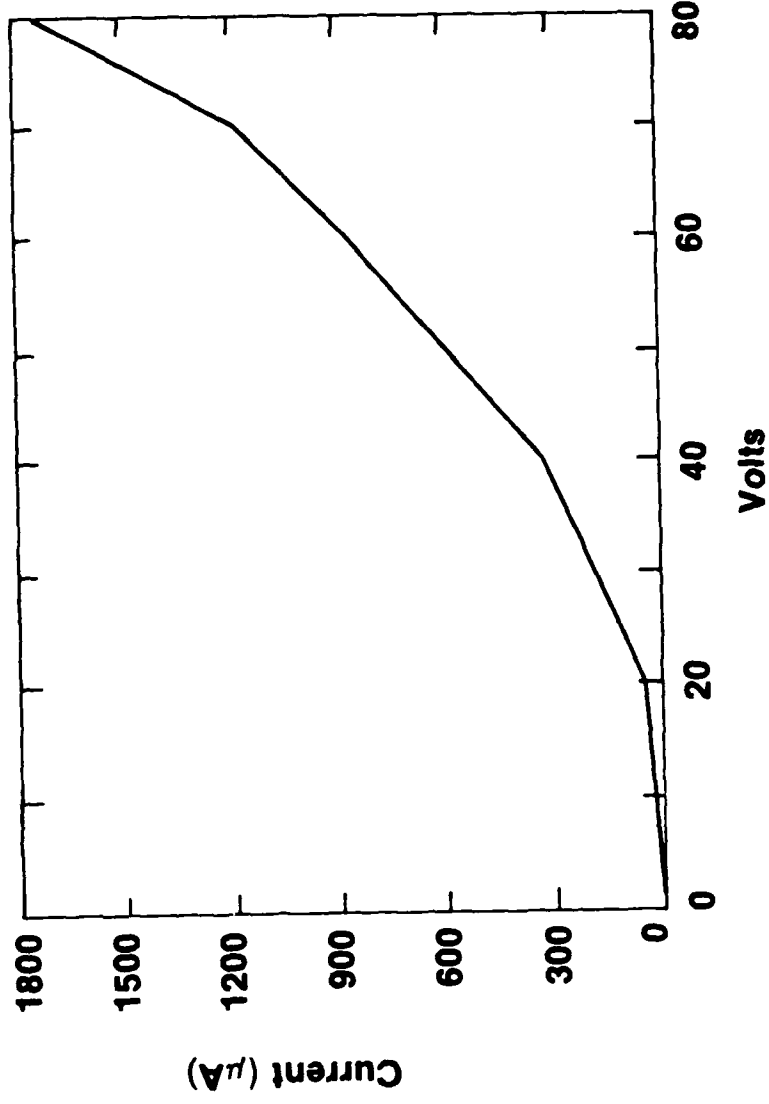
100- μm
spot separation

200- μm
spot separation

E3591

**I-V Characteristic of Al Evaporated on Si
2-mm Gap**

UR
LLE



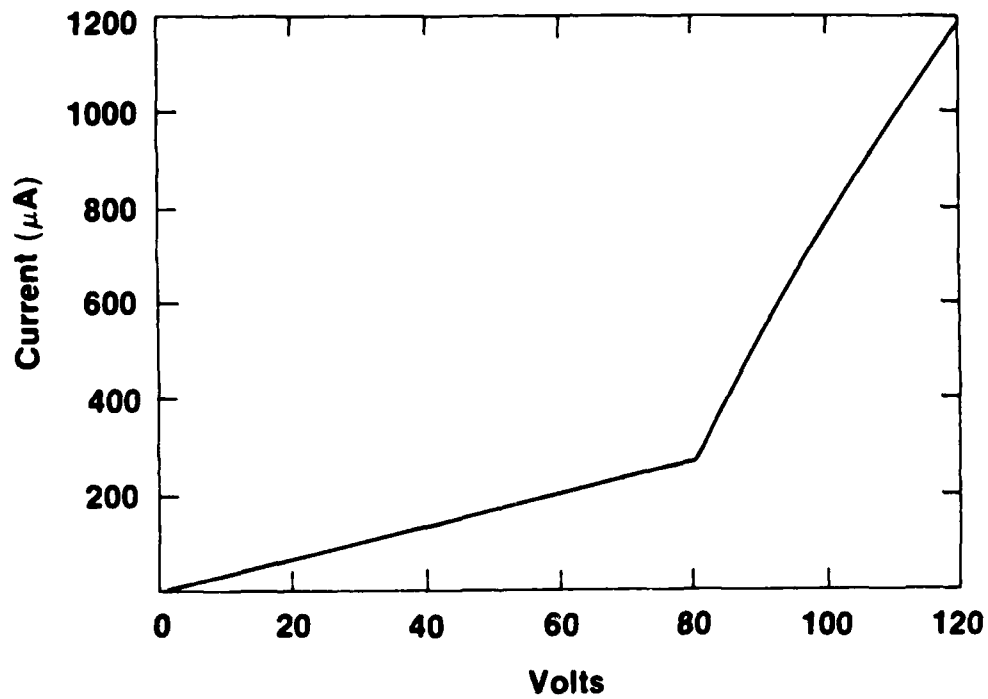
The nonprocessed contact is not ohmic.

E3592

Fig. 3

I-V Characteristic of Laser-Annealed Au on Si 2-mm Gap

UR
LLE 

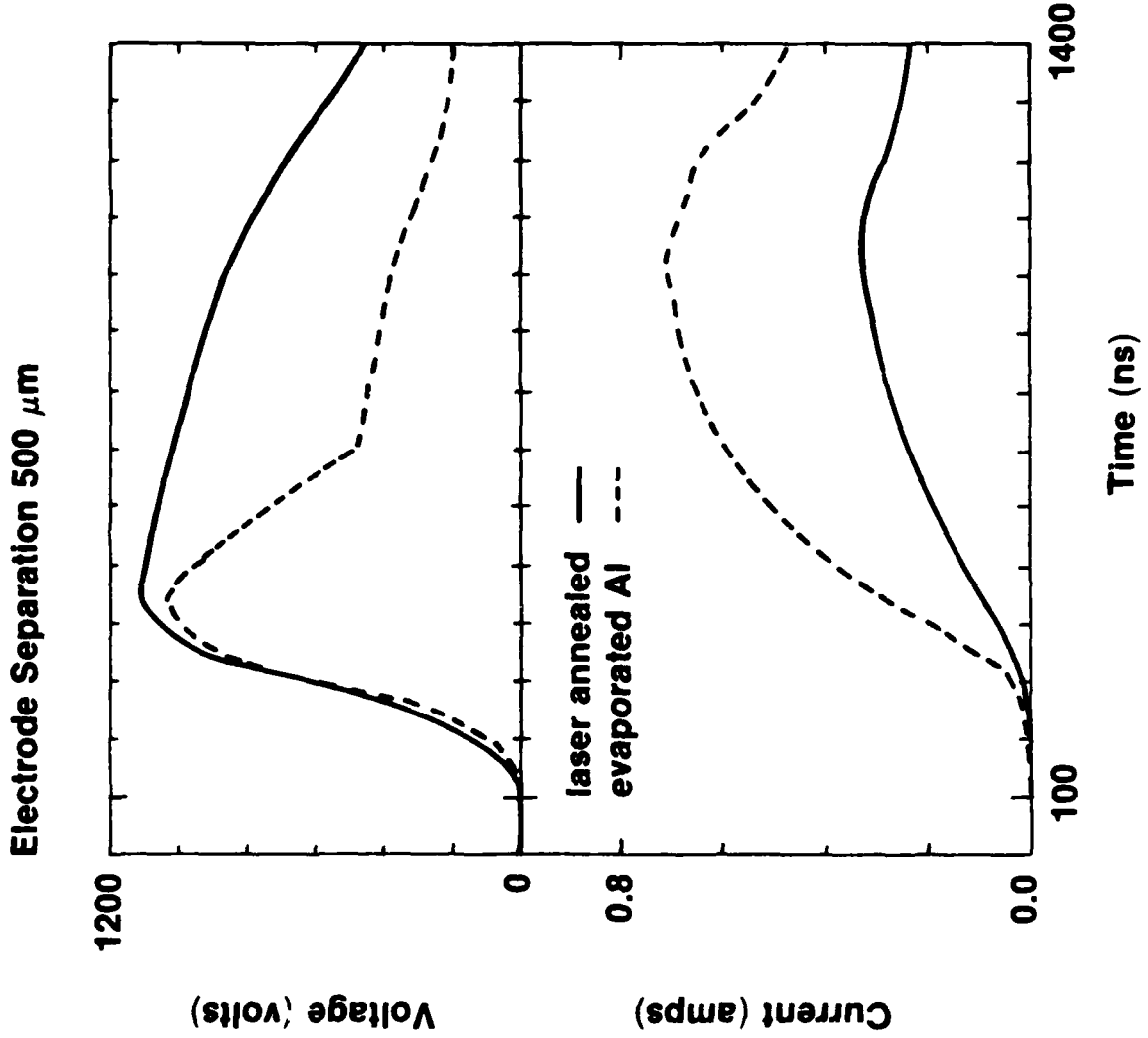


At 80 V the laser-annealed contact switches from the ohmic to injected current regime.

E3593

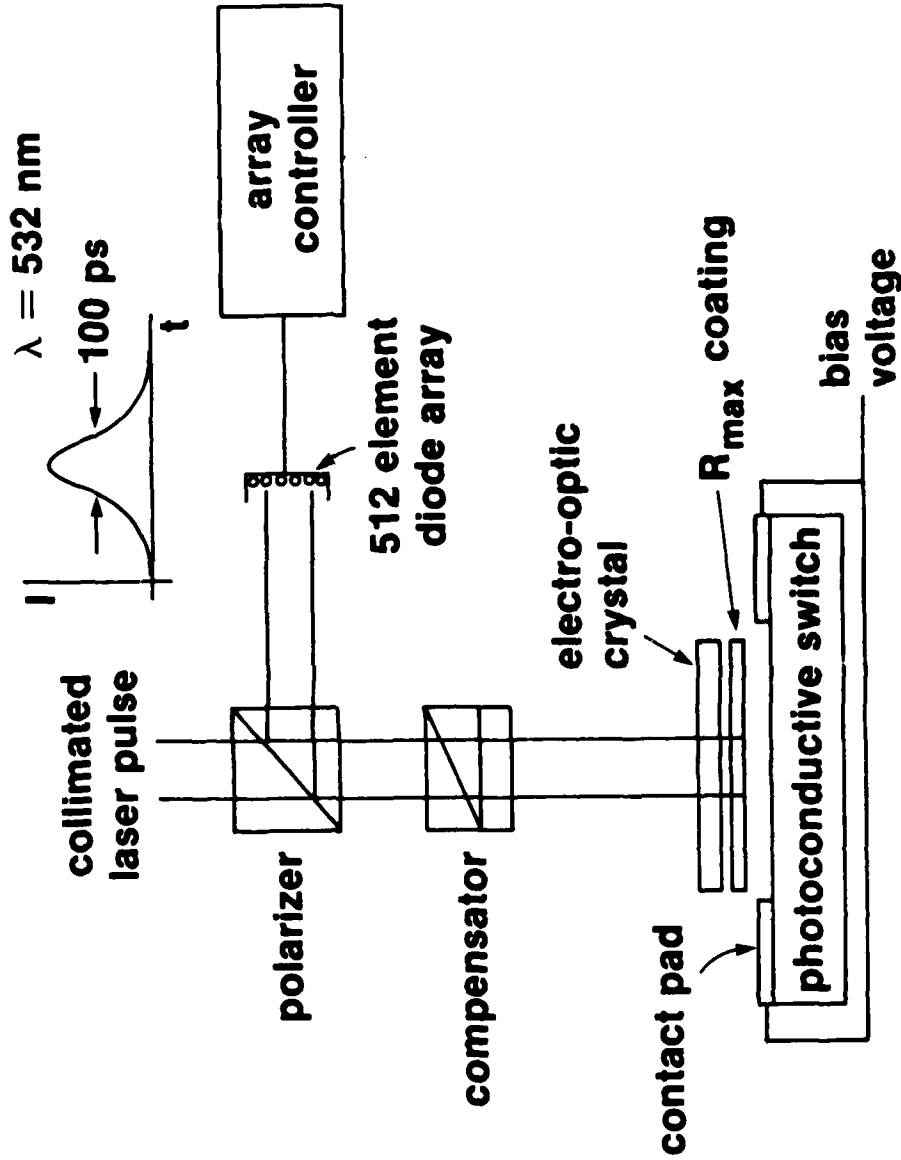
Pulsed-Leakage Current and Bias Voltage of Si Switches

UR
LLE



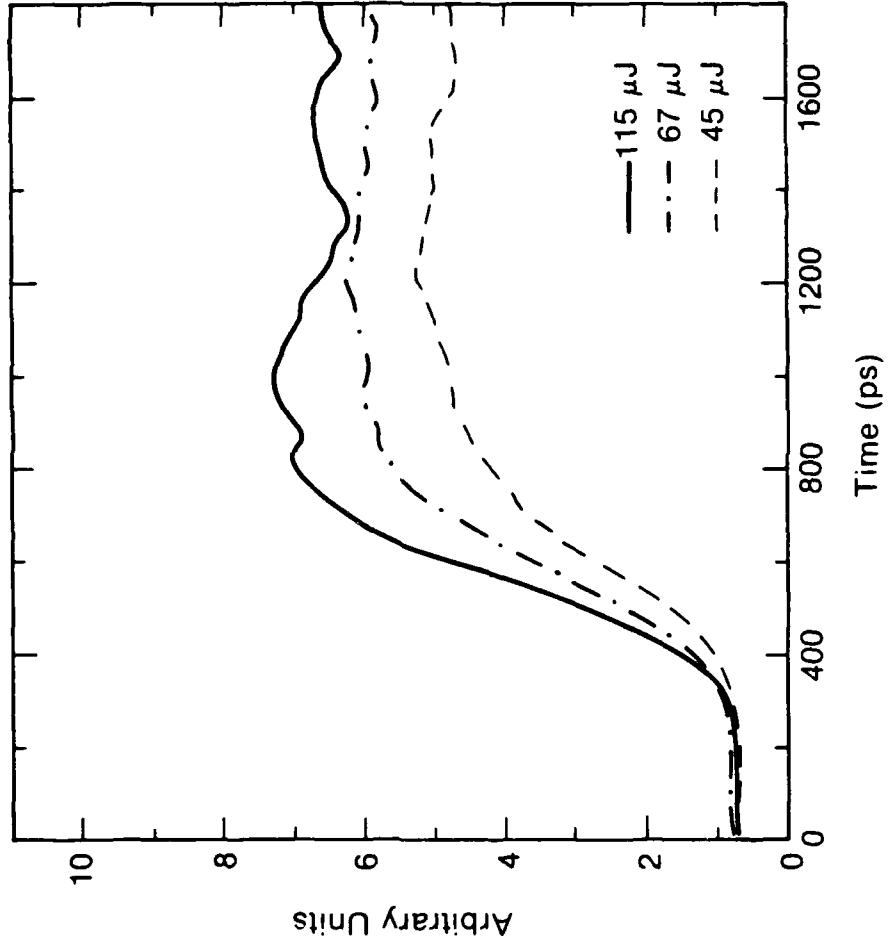
Surface-Field Imaging Apparatus

UFR
LLE



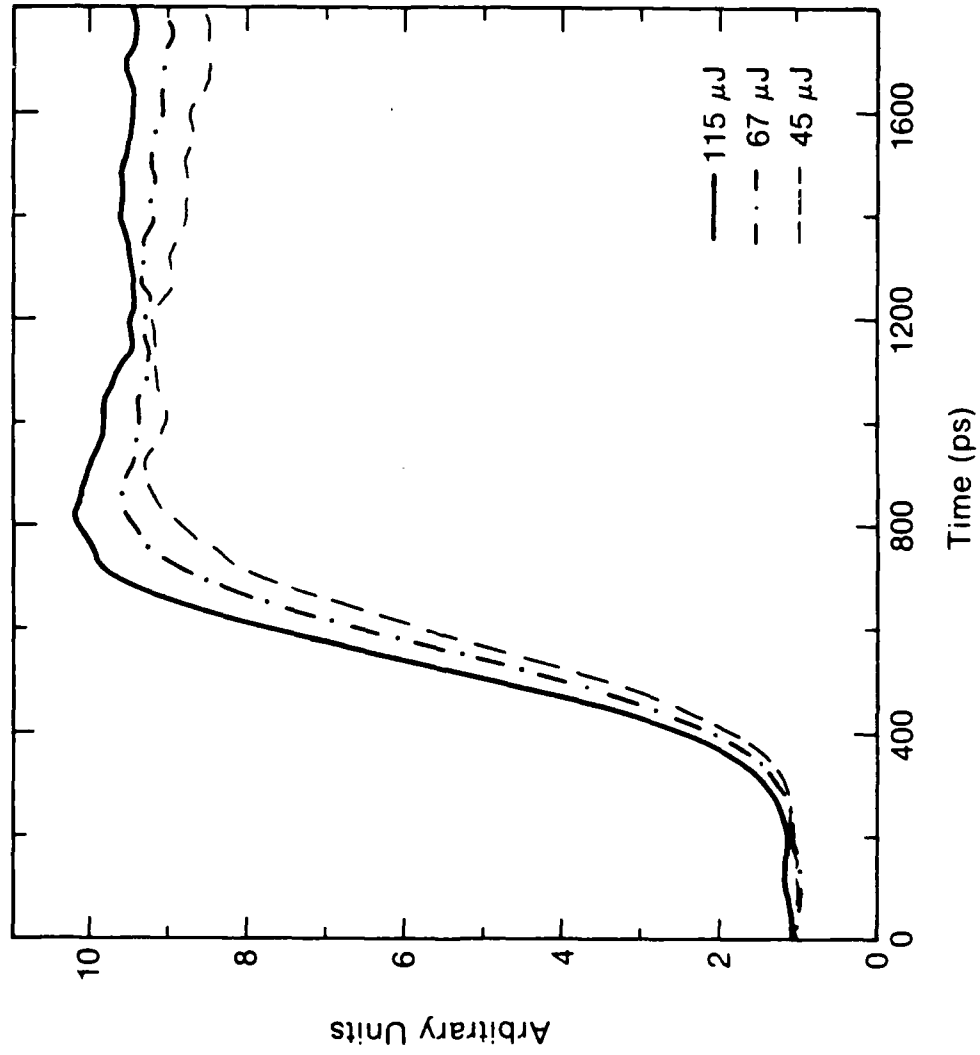
Z499

Rise Time of Si Photoconductive Switch Biased at 13 kV
at Various Optical Energies



Z554

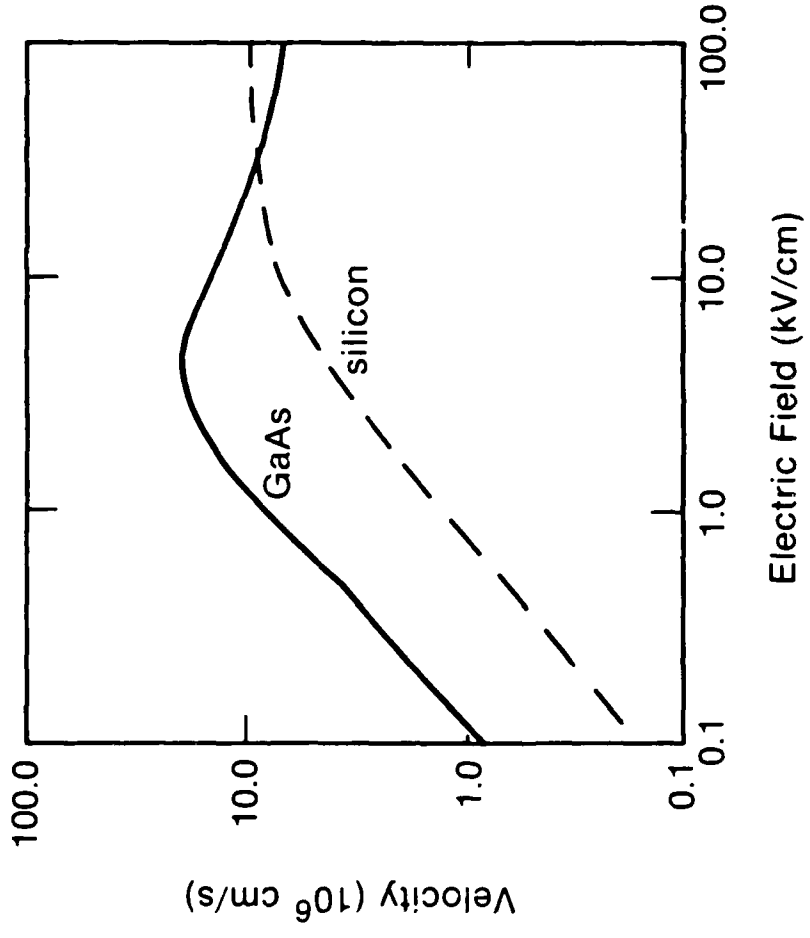
Rise Time of Si Photoconductive Switch Biased at 19 kV
at Various Optical Energies



Z555

Electron Velocity in Si and GaAs versus Electric Field

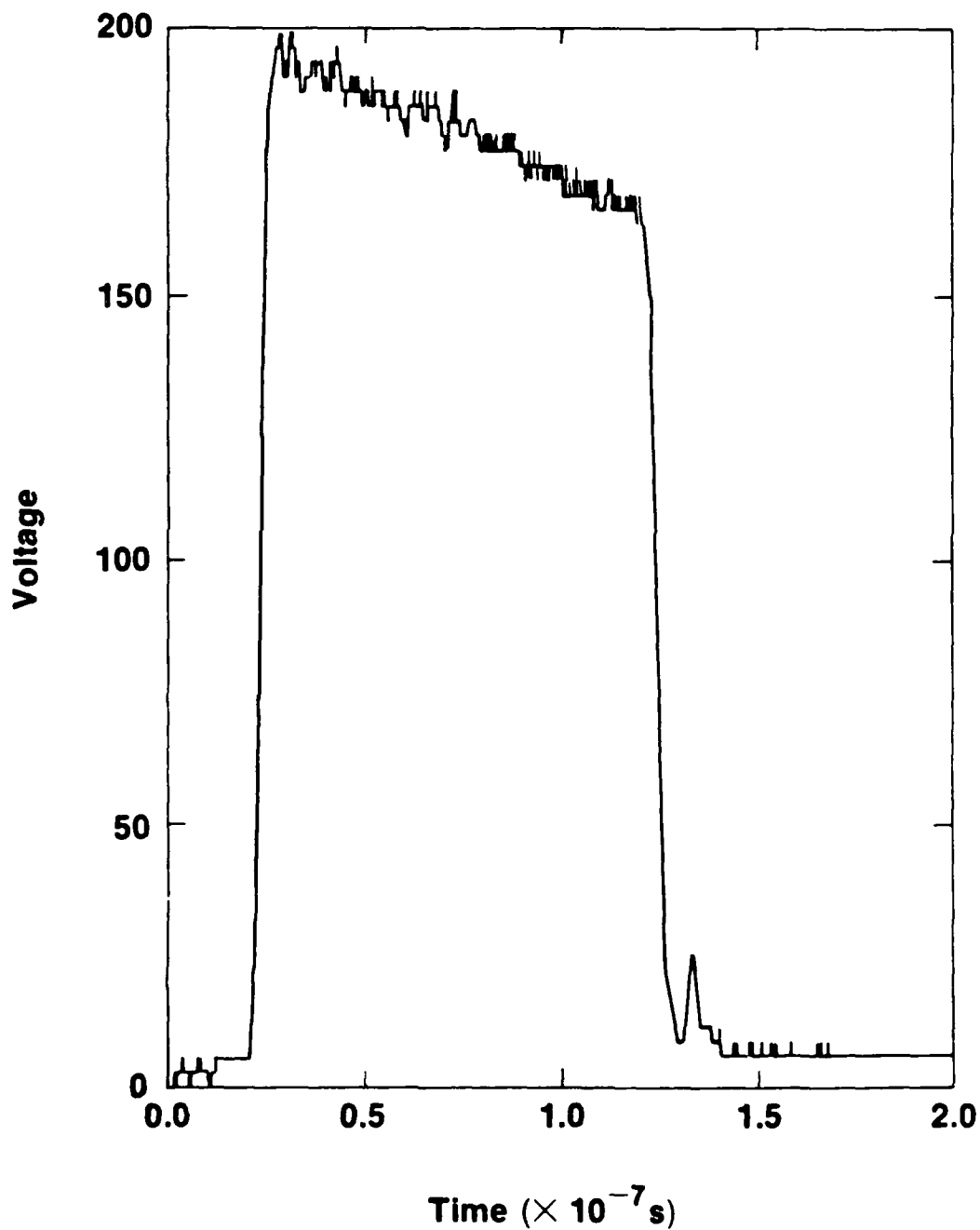
UJA
LLE



Z485

Decay of Photoconductivity

UR
LLE 

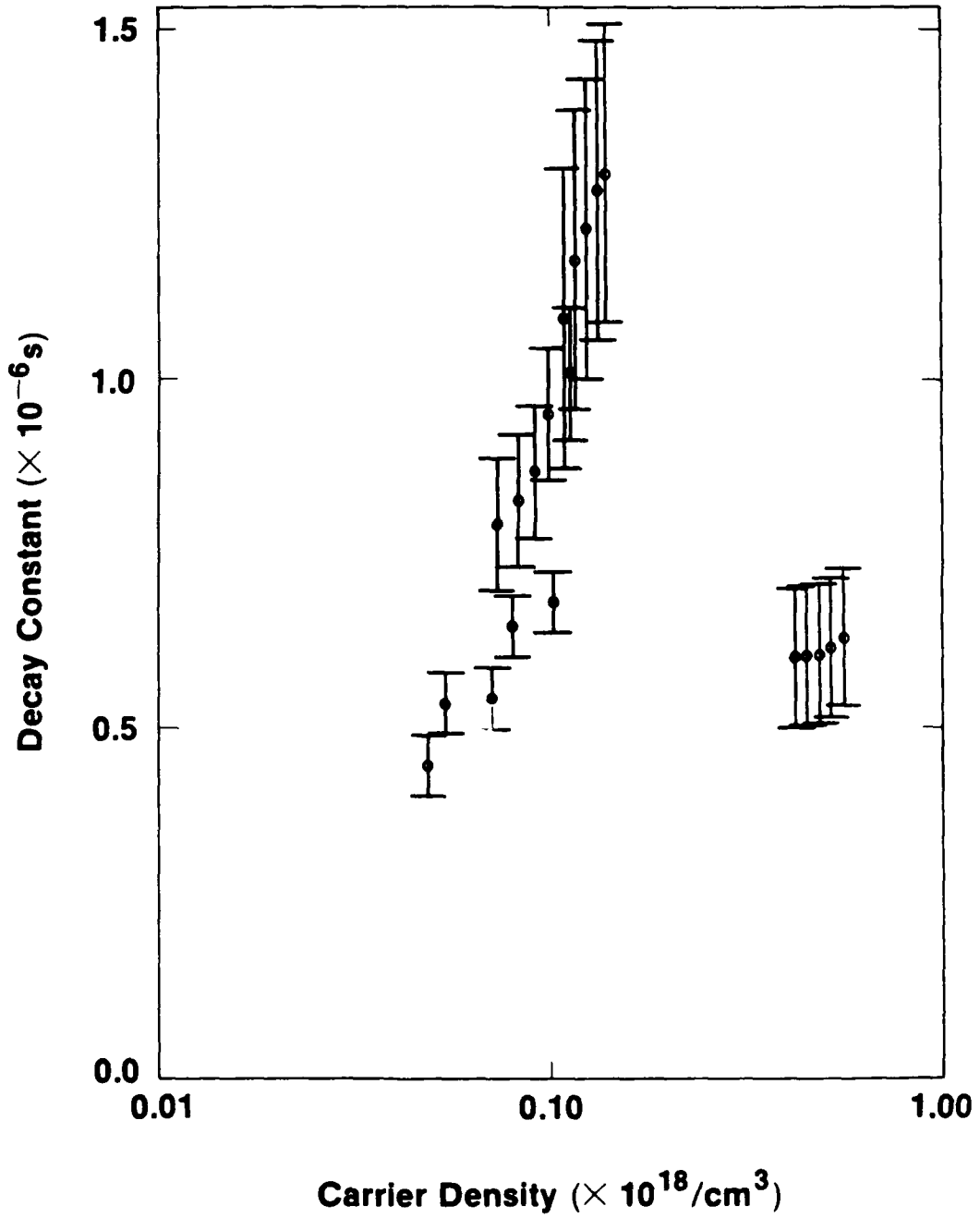


Z172

Fig. 10

Fast Component of Photoconductivity Decay vs Carrier Density

UR
LLE 

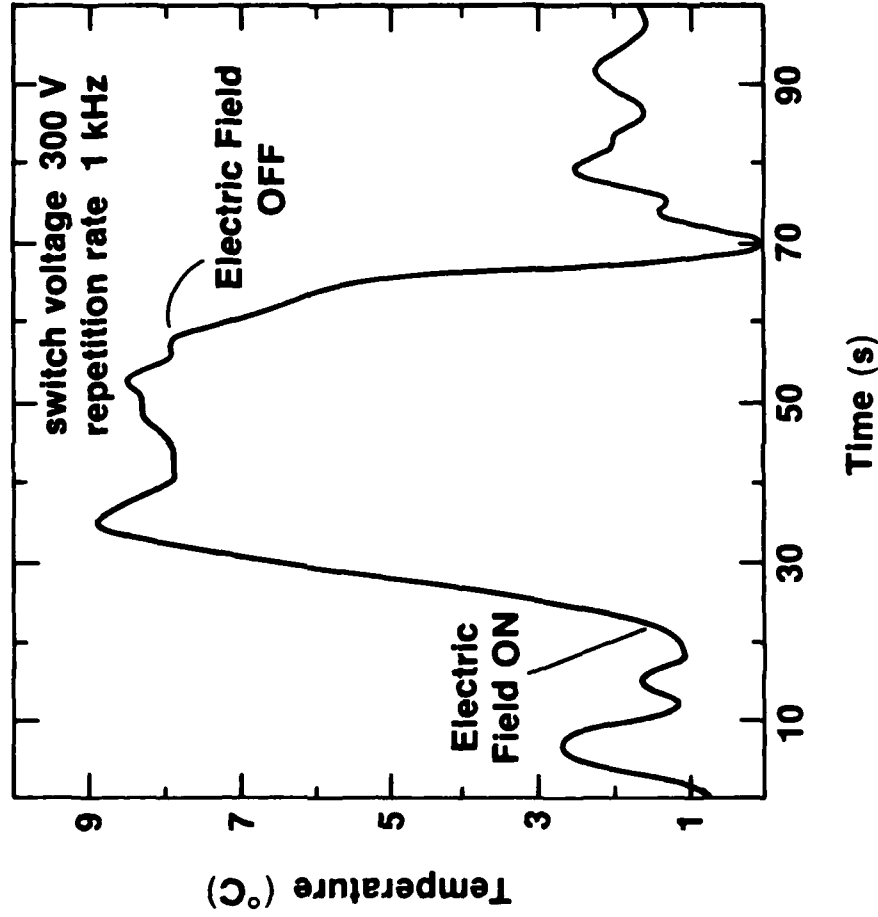


Z174

Fig. 11

Temperature Rise in a Photoconductive Switch Operating as Measured by the Transmission of the Optical Trigger Pulse

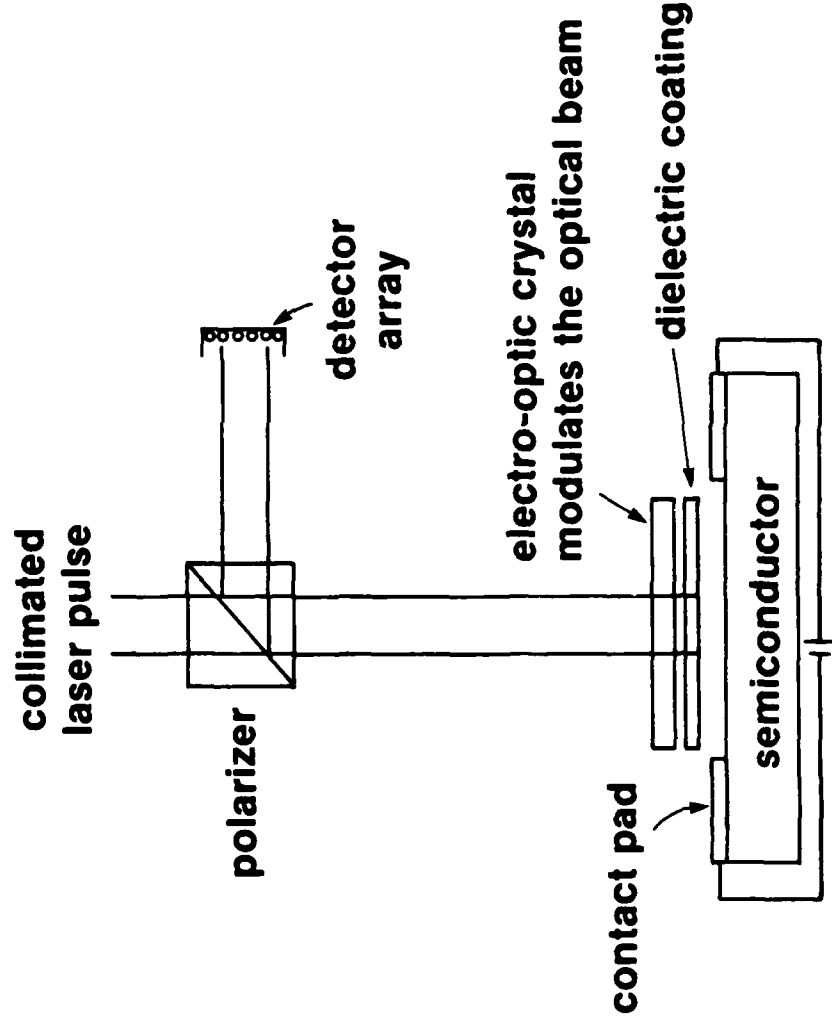
UFR
LLE



Investigation of Surface Breakdown Using Optical Probes University of Rochester



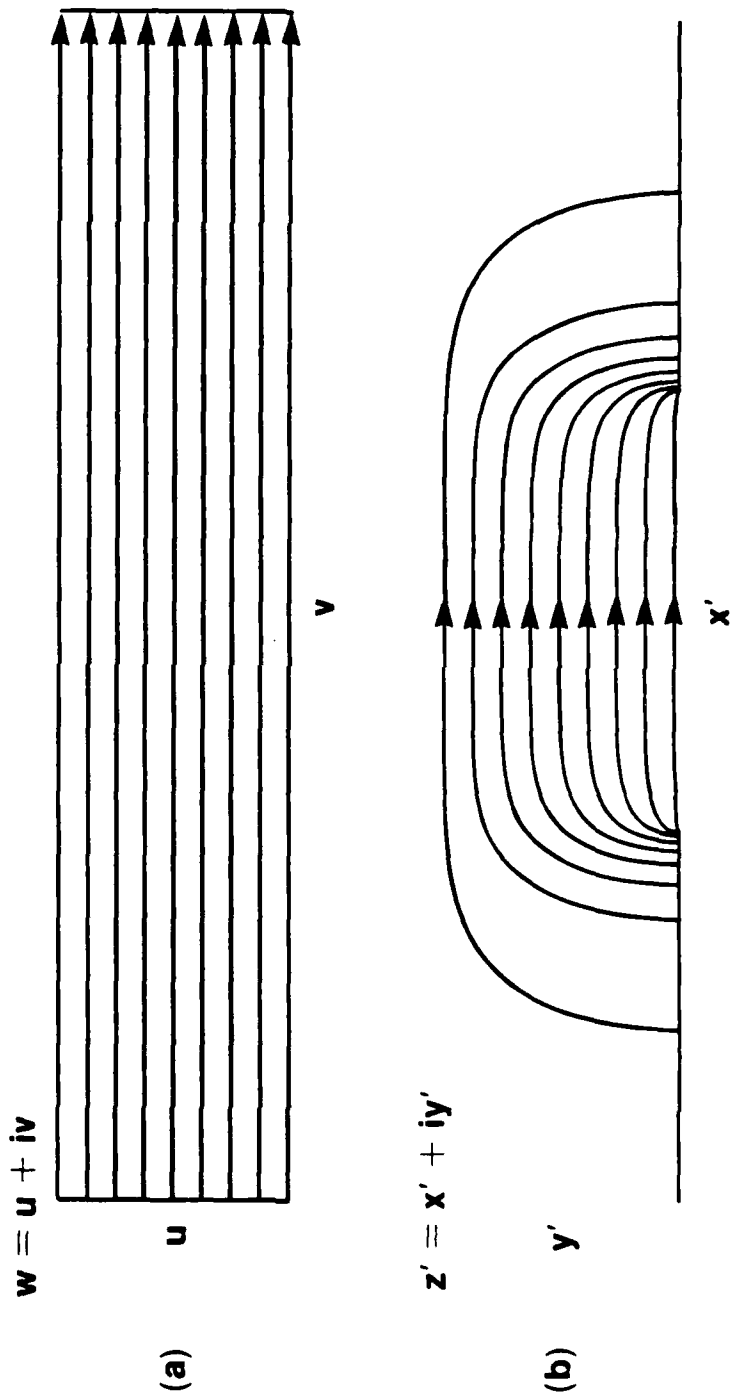
Apparatus for Producing a Time-Resolved Optical Image of the Surface Electric Field on a Semiconductor



Z608

Conformal Mapping of Parallel-to-Coplanar Electrodes

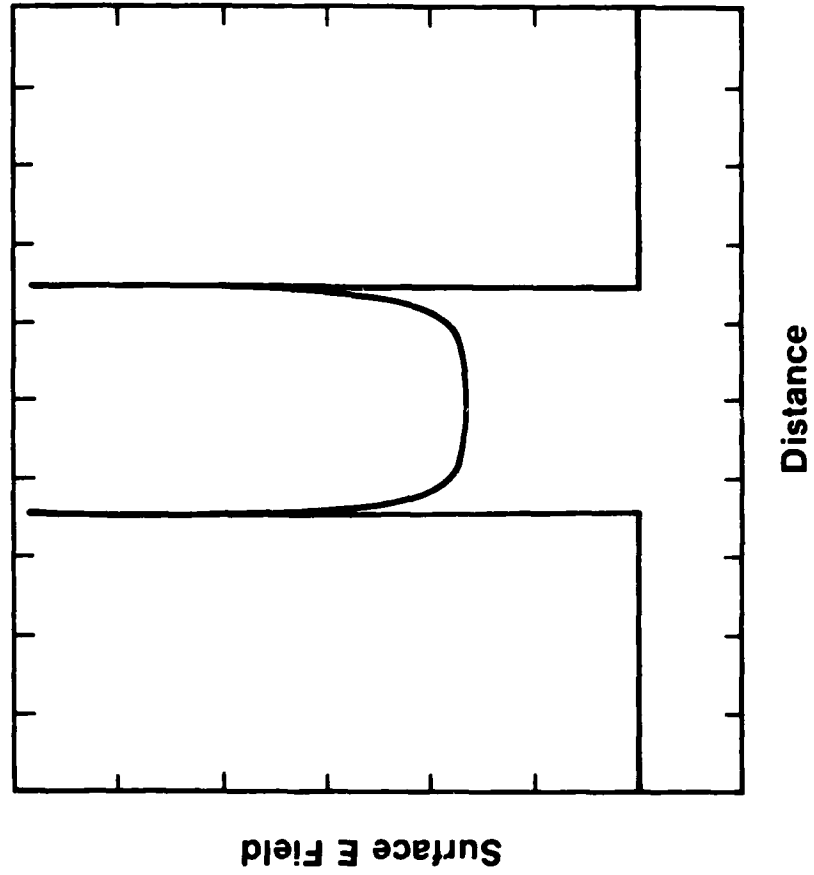
UJF
LLE



Z434

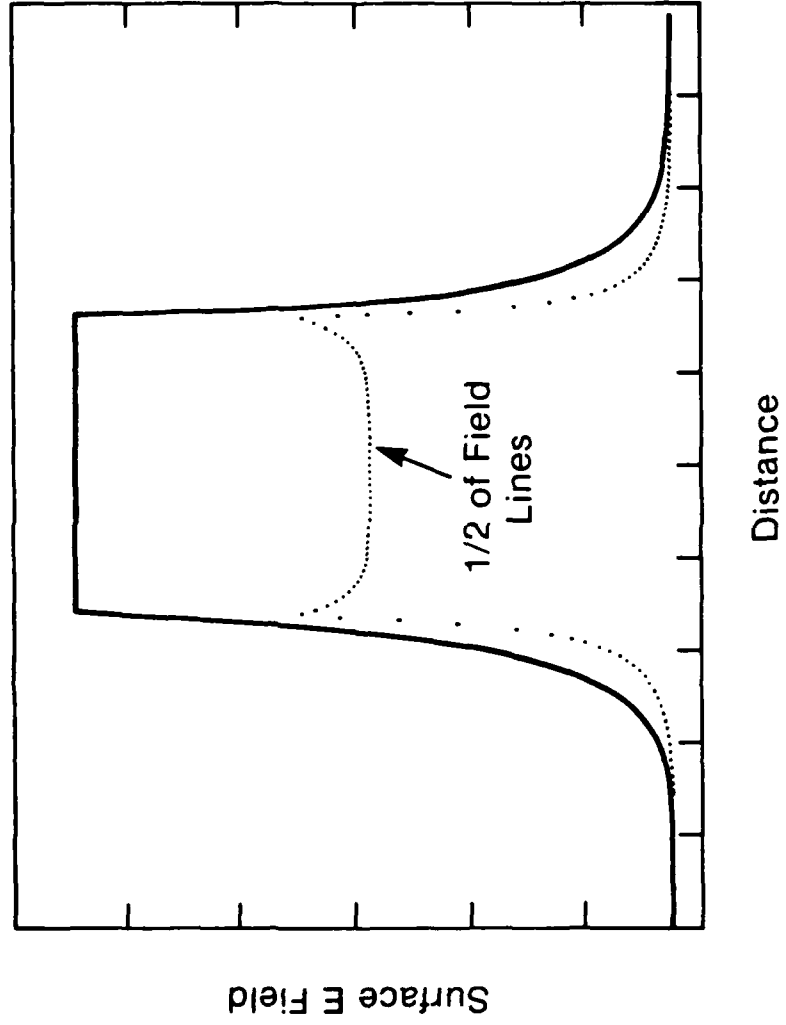
Electric Field in the Plane of Coplanar Electrodes

UR
LLE



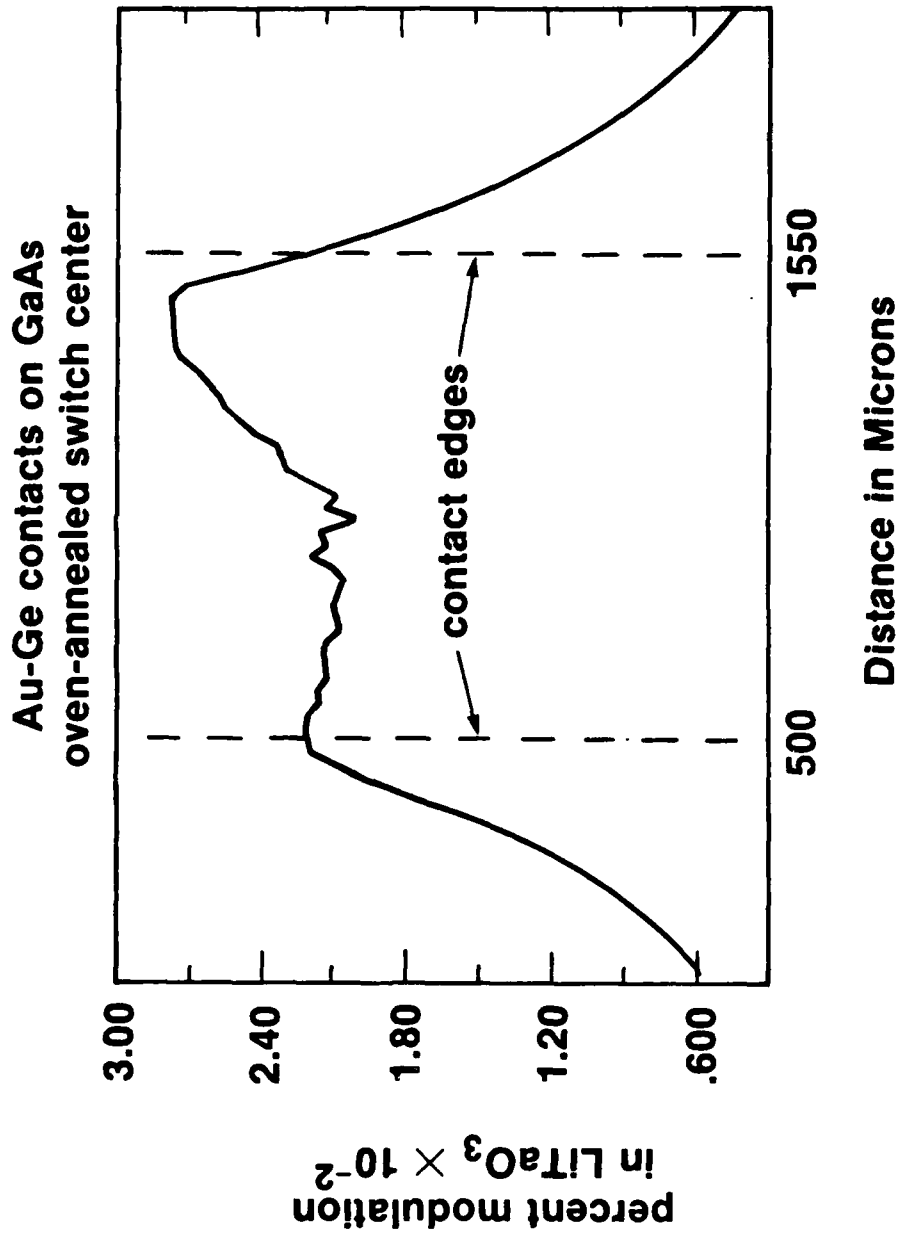
Z435

Integrated Surface Electric-Field Profile



Z428

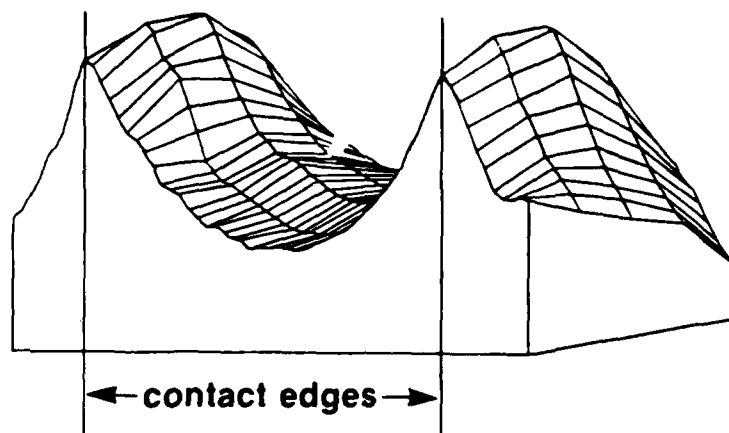
Surface Field Profile
UR
LLE



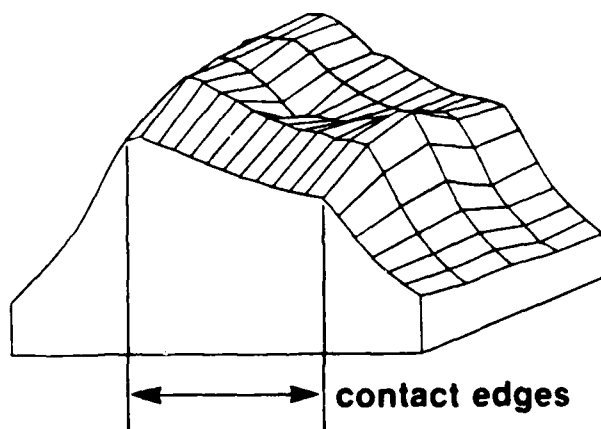
Z274

Surface Field Profiles for GaAs

UR
LLE 



**Indium Contacts on GaAs
(unannealed)**

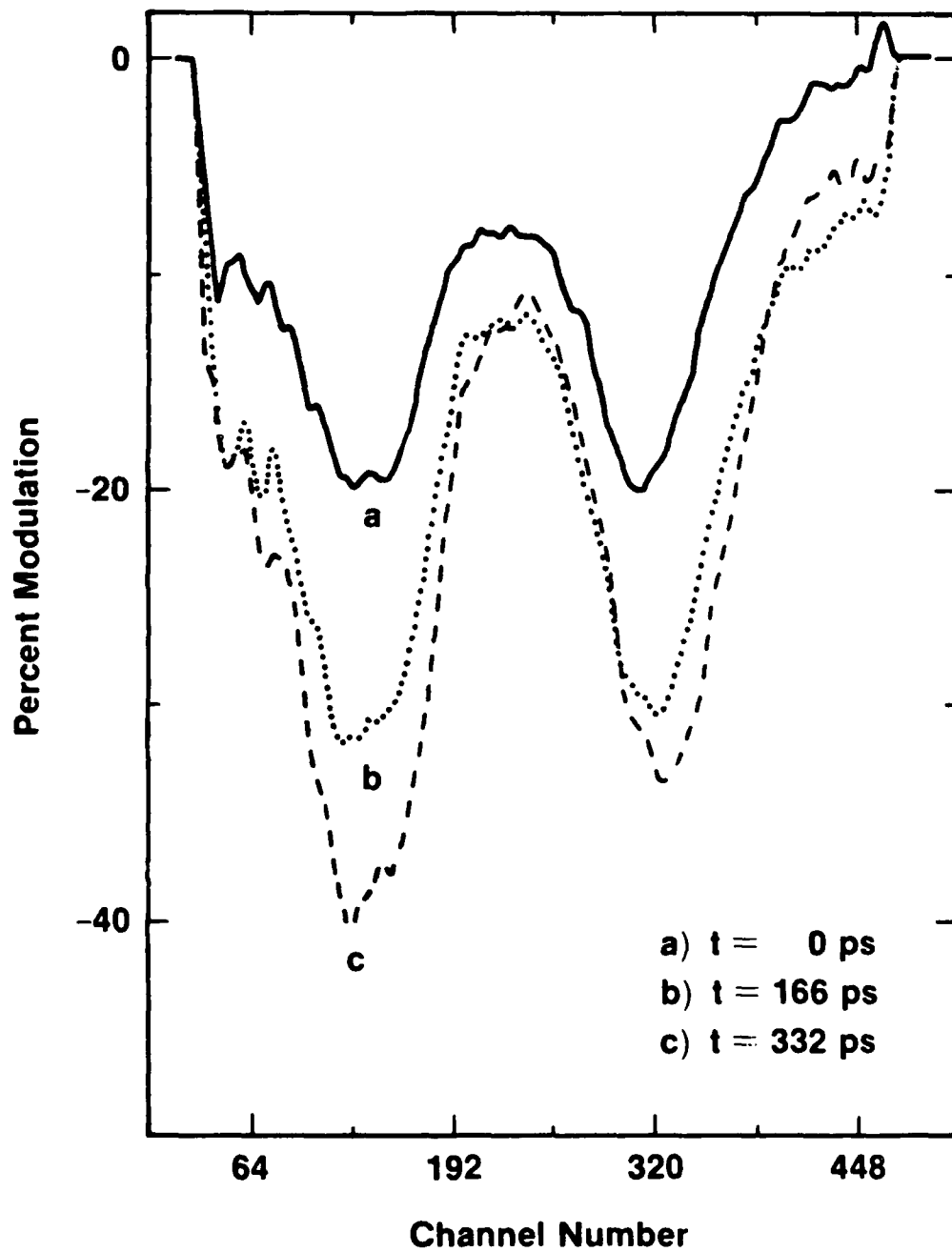


**Au-Ge Contacts on GaAs
(annealed)**

Z280

Surface Electric Field on Si versus Time Bias 1 kV; Gap 2 mm

UR
LLE 

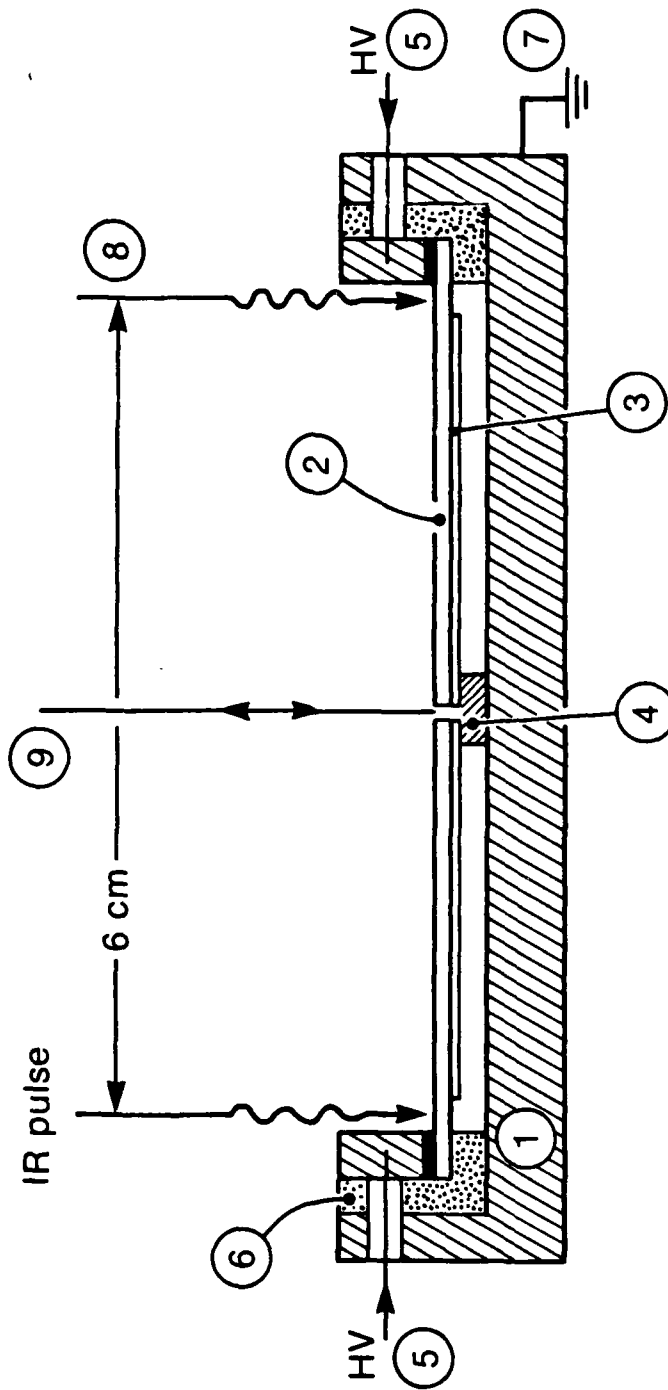


Z426

Fig. 19

Cross Sectional View of an Optically Switched
Radial Transmission Line

UR
LLE



Z362

Tempora! Profile of Pulse in an Accelerator Structure



Field versus Time for Various Radii

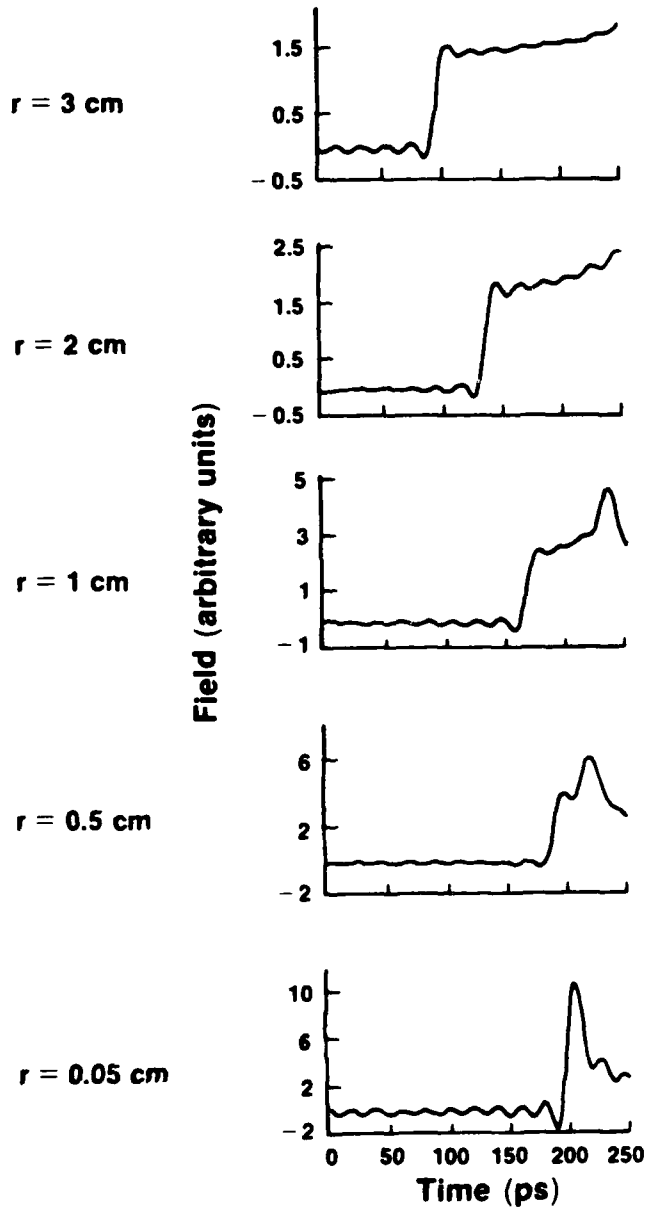
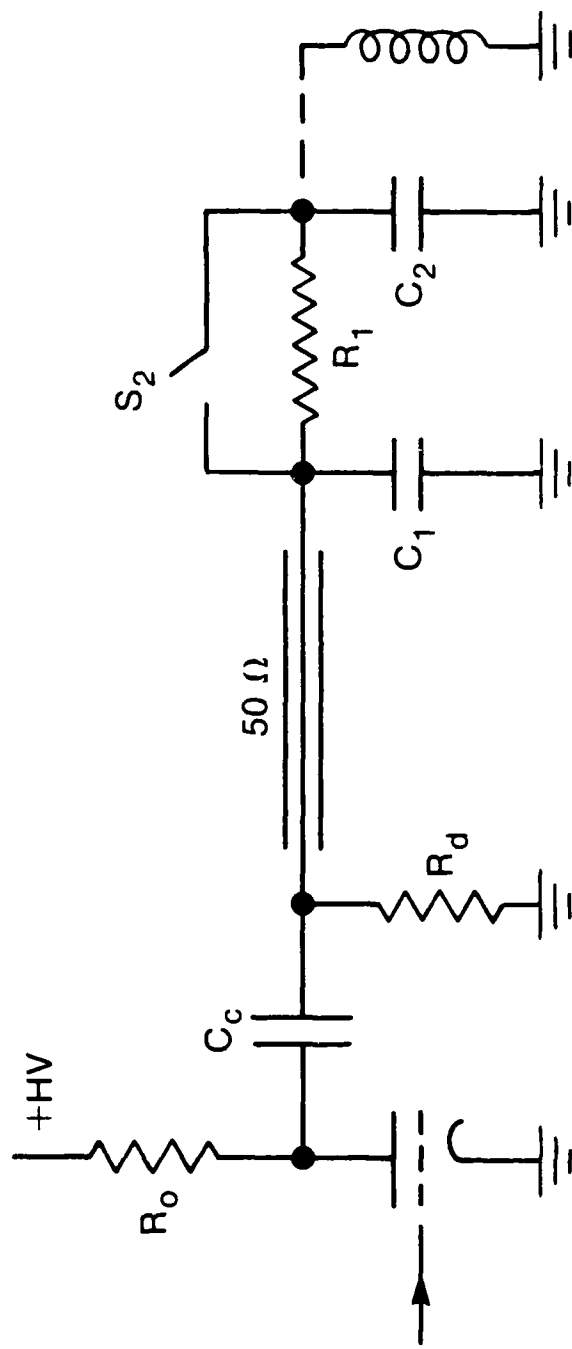


Fig. 21

Equivalent Circuit for a Radial Transmission Line and Driver

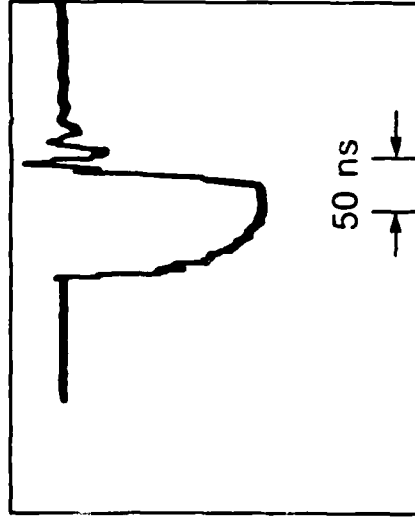
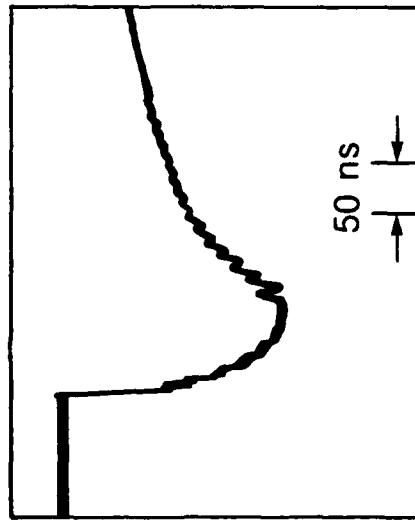
UR
LLE



Z363

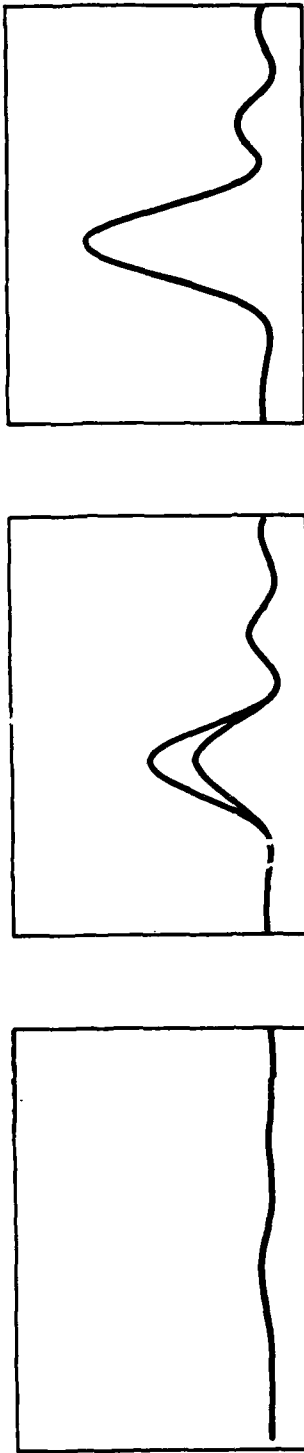
Voltage Waveforms at the Rim of a Radial Transmission Line

UR
LLE



Z364

Electro-Optic Signal at the Center of a Radial
Transmission Line



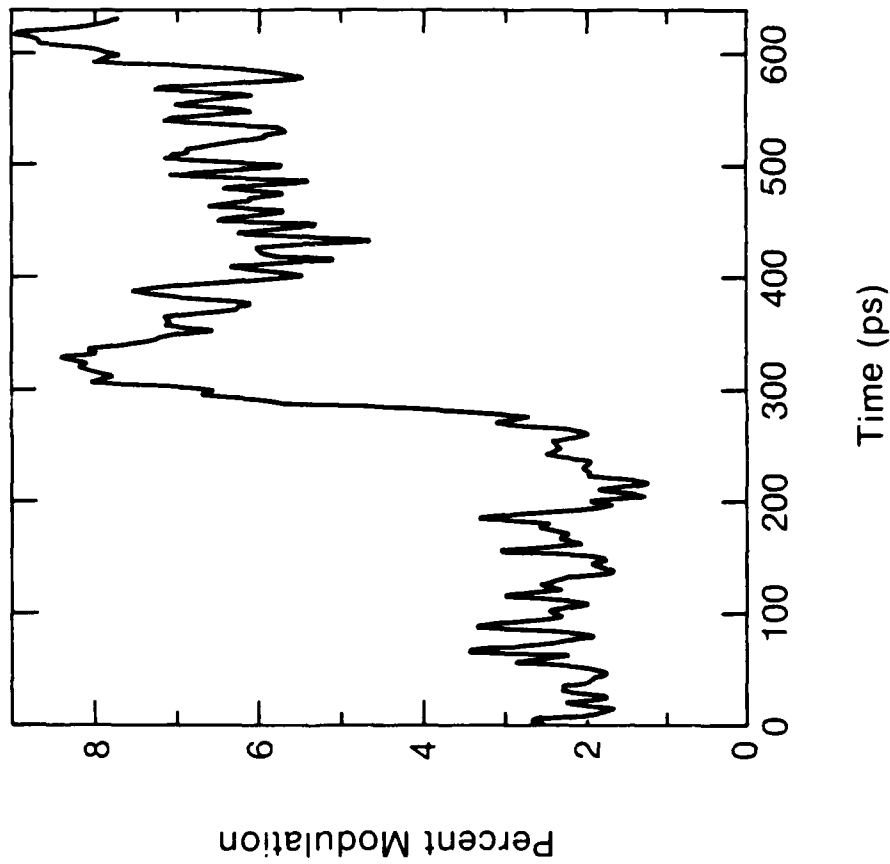
(a) $\phi = 0^\circ$

(b) $\phi = 45^\circ$

(c) $\phi = 90^\circ$

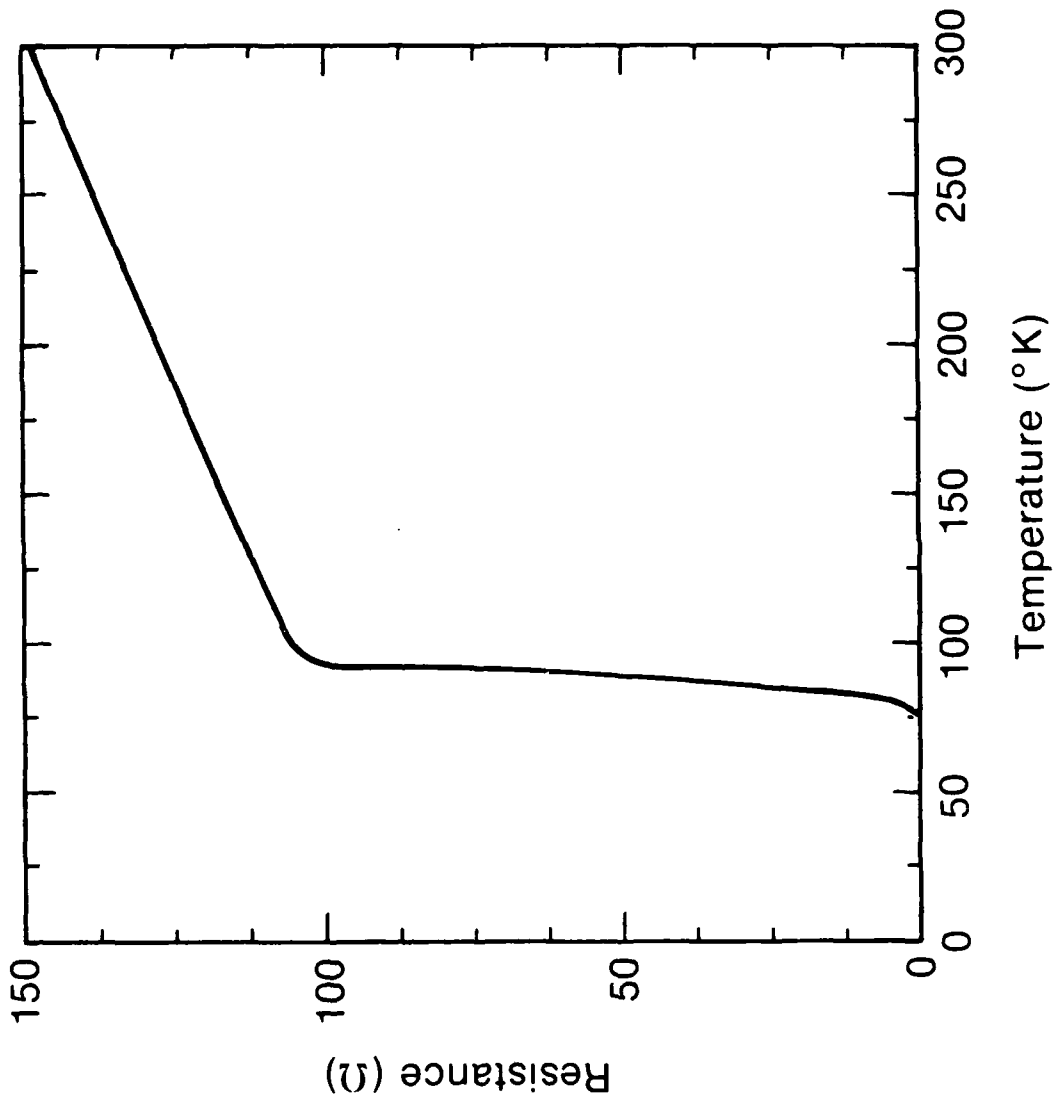
Z367

Rise Time of a High-Voltage Photoconductive
Pulse on a Radial Transmission Line



Z341

Resistance versus Temperature for YBCO Opening Switch



EQUILIVANT CIRCUIT OF YBCO SWITCH

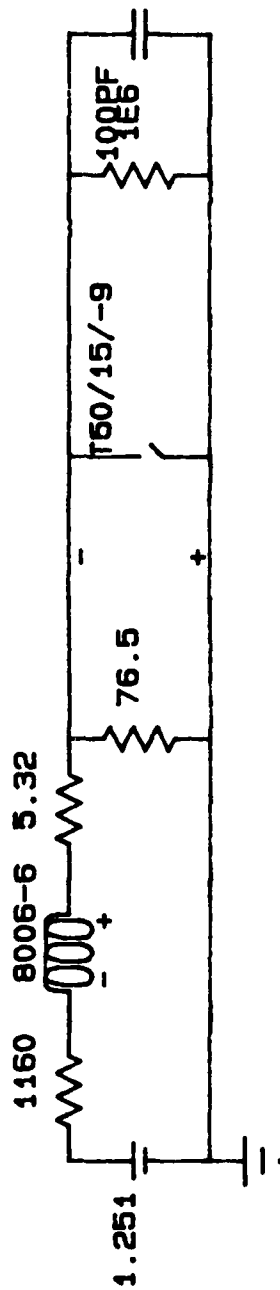
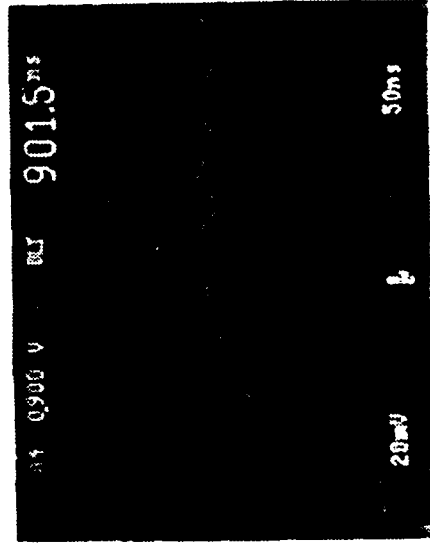


Fig. 27

Optically Activated Thin Film YBCO Opening Switch

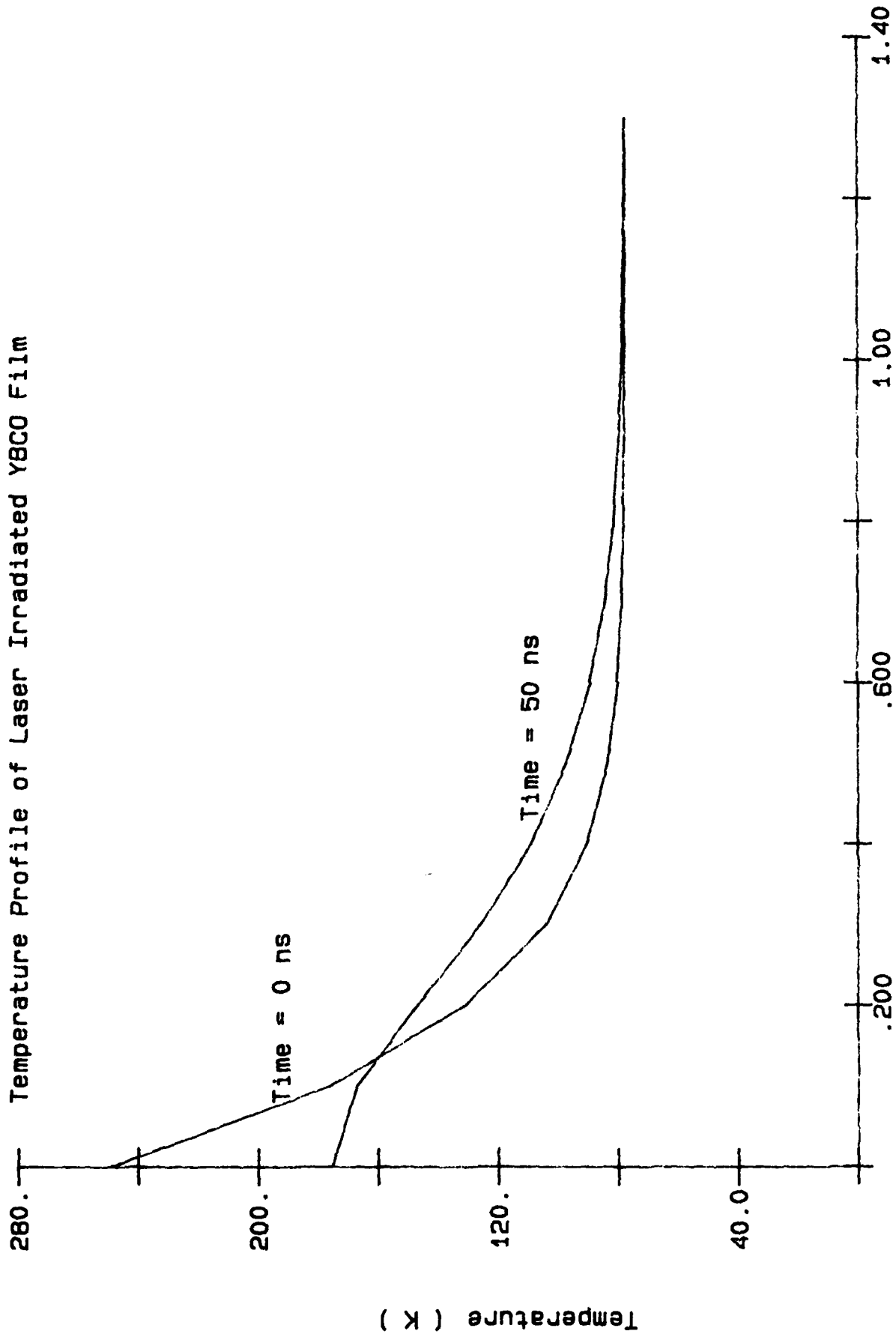


load voltage implies a change
in resistance from
superconducting to 71Ω

laser illumination
(4.7 mJ/cm^2 , 52 Hz, 200 ps)

Z613

Temperature Profile of Laser Irradiated YBCO Film



Distance (microns)

Fig. 29